Contents — L through O

THE LACUSTRINE RESERVOIRS IN HELLAS IMPACT BASIN REGION. H. Lahtela[1], V.-P. Kostama[1], M. Aittola[1], T. Öhman[2] and J. Raitala[1]. [1]Planetology Group, Department of Physical Sciences, P.O. Box 3000, FIN-90014, University of Oulu, Finland, <hlahtela@paju.oulu.fi>, [2]Institute of Geosciences, Department of Geology, P.O. Box 3000, FIN-90014, University of Oulu, Finland.

Introduction: The Hellas Basin in the southern hemisphere of Mars has a depth of ~9 km and a diameter of ~2000 km [1], which makes it one of the largest multi-ring impact basins in the solar system [2]. The impact itself could have been an oblique one with a trajectory from NW [1,3,4]. Despite numerous evidences (deeper excavation and steeper walls on the uprange profile, higher and more densely concentrated massifs in the downrange rim lobe, etc. [3,4]) for this hypotheses, it still must be considered as speculative.

Hellas' influence on the evolution of Mars since the basin's formation in the Early Noachian [e.g. 1] has been enormous. An obvious outcome of the impact are concentric and radial fractures and graben, which have in turn affected e.g. drainage patterns [5,6] and the morphology of younger craters [7]. It has also been suggested that the formation of volcanic paterae and associated plains on the NE and S rims of Hellas basin [4,5,6,8] and even the enigmatic volcanic region around Alba Patera antipodal to Hellas [9,10] might have been controlled by the Hellas impact. Hellas influences also the modern-day Mars, since numerous regional and global dust storms originate from the Hellas region [11]. All these processes result in a geologically versatile region [e.g. 12] which is seen, for example, in the diverse crater population [13].

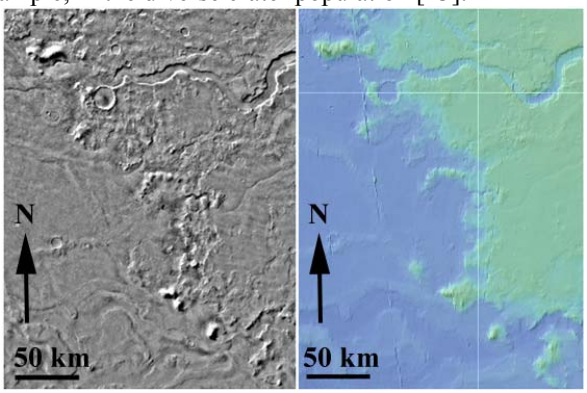

Figure 1. The possible shoreline in the eastern rim of Hellas. (Left: Viking MDIM; Right: MOLA topography).

Fluvial activity: Hellas area is rich in details of fluvial formations. Although a wide variety of different channels implying fluvial activity can be observed on both sides of Hellas, particularly the low eastern plains region bears softened features adjacent to large channel formations. This activity has probably contributed to the fact that the eastern rim of Hellas has been practically eroded away.

The most notable evidence of erosion are the large outflow channels east of Hellas. It has been suggested that the origin of these channels would be the late-stage effusive volcanism of the Tyrrhena Patera [14], which triggered collapse and outflow erosion, producing the Dao, Niger and Harmakhis Vallis. In addition to these three, we have the joined Reull and Teviot Vallis. The Dao and Harmakhis Vallis change radically in morphology at the "shoreline" scarp of Hellas, which is also a distinct change in regional topography (Fig. 1). They both transform from sharp and exposed features into diminished and partly buried. In this they closely resemble the terrestrial marine channels, which continue beyond the mouths of large rivers.

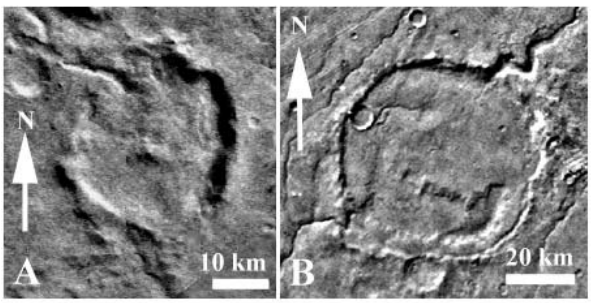

Figure 2. Hellas crater lakes. Closed (A) and open system (B).

Within Hellas region there are also several larger craters and depressions which show interaction by post-impact fluvial activity. In addition to the erosion effects of the channels flowing through the crater, they may also deposit material into the craters. This is especially true when many of the craters described above have been temporary water reservoirs during the period of time when the inflow has partially filled them and before the water level rise has given way to the outflow channel formation. Depending on the amount of water and erosion and also on the repeated occurrence of the inflow involved, this lacustric phase has resulted in layered sediments on the crater floor. This process smoothens the crater interiors and may create deep water-saturated layered materials for the subsequent permafrost formation. The existing permafrost may further add debris apron type mass movements inside the crater rims.

Crater lakes and other reservoirs: The crater lakes of Hellas region are one of the most prominent

features of lacustric processes. They are identified by inflowing rim channels. The crater lakes are either closed systems with only an inlet channel (Fig. 2a) or open systems with the additional outlet channel [15] (Fig. 2b). In cases, where there is at least two craters connected by same channel, a lake chain is formed (Fig. 3a). We also have layered deposits and smooth floors within other depressions such as the Teviot Vallis (Fig. 3b). Distribution of these reservoirs is shown in Fig. 4.

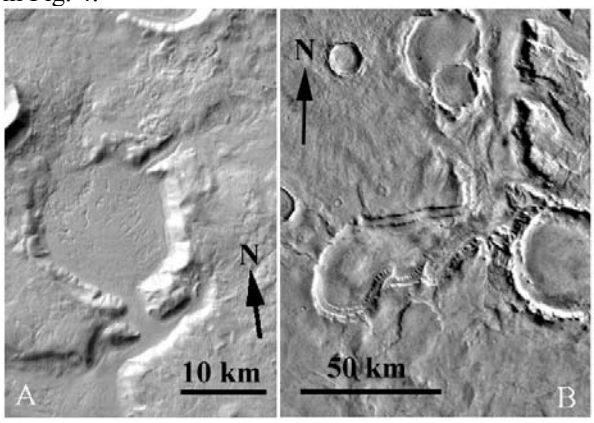

Figure 3. A. Possible crater lake chain adjacent to the Reull Vallis. B. Teviot Vallis reservoir.

Together with the decreasing inflow into the crater its sedimentation effect also diminishes. The final phase which still carries some amount of solid material to deposit, is seen as a delta formation [15]. In some cases a wider and thinner delta layering may be visible, possibly due to a stronger final inflow pulse.

The deposits can also be found at the very bottom of Hellas basin itself. These sediments are later modified by polygonal structures. These structures as well as the possible shorelines (Fig. 1) are evidence of a great, ancient lake within the rims of the crater.

Conclusions: Hellas region is rich in both fluvial and lacustrine formations. As seen from the distribution of the possible reservoirs, they are extinct within the volcanic regions of Malea and Hesperia Planum. Concentration seems to be to the eastern outflow channels and to the north of Hellas basin itself, which could have functioned as a lake also at some point. Studies of these "reservoirs" will reveal additional details of Martian erosion, deformation and sedimentation within the craters and other depressions.

References: [1] Leonard G. J. & Tanaka K. L. (2001) Map I-2694, USGS [2] Spudis, P.D. (1993) Geology of Multi-ring Impact Basins, (1993) Cambridge, 263 pp [3] Leonard G.J. & Tanaka K. L. (1993) *LPS24*, 867-868. [4] Tanaka and Leonard G.J. (1995) *JGR 100*, 5407-5432. [5] Wichman, R.W. and Schultz, P.H., (1989) *JGR 94*, 17333-17357. [6] Crown D. A. et al. (1992) Icarus 100, 1-25. [7] Öhman, T. et al. (2003) *LPS34*, Abstract #1311. [8] Peterson J. E. (1978) *LPSC9*, 887-888. [9] Peterson J. E. (1978) *LPS9*, 885-886. [10] Williams D. A. & Greeley R. (1994) Icarus 110, 196-202. [11] Martin, L.J., & R.W. Zurek, (1993) *JGR 98*, 3221-3246. [12] Kostama, V.-P. et al. (2002) *LPS33*, Abstract #1486. [13] Aittola, M. et al. (2002) *LPS33*, Abstract #1485. [14] Carr, M.H. & Schaber G.G (1977) *JGR 82*, 4039-4054. [15] Cabrol, N. A. & Grin, E. A. (1999) Icarus 142: 160.

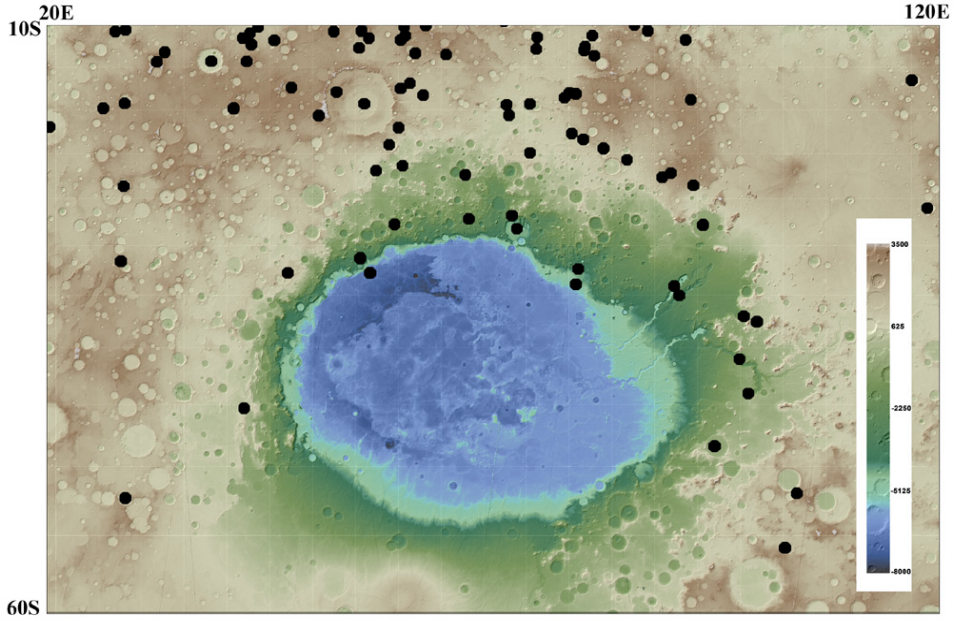

Figure 4. The Hellas impact basin topography (MOLA) and the "reservoirs" located within the region. Notice the continuous shoreline in pale green and the sharp depression around the Alpheus Colles plateau within the basin itself.

FIRST OBSERVATION OF SILICATE HOLLANDITE IN A TERRESTRIAL ROCK. F. Langenhorst[1] and B. Dressler[2], [1]Bayerisches Geoinstitut, University of Bayreuth, D-95440 Bayreuth; Falko.Langenhorst@uni-bayreuth.de, [2] 185 Romfield Circuit, Thornhill, Ontario, L3T 3H7; burkhard@attcanada.ca

Introduction: At high pressures in excess of 10 GPa, feldspars undergo phase transformations to hollandite-structured polymorphs [1]. Such silicate hollandite is expected to occur in subducted oceanic slabs at inaccessible depth in Earth´s mantle but it can also occur in the context of bolide impact events. In fact, silicate hollandite has recently been discovered in shock veins of heavily shocked ordinary chondrites [2-4] and the SNC achondrite Zagami [5,6] but so far it has never been reported for a terrestrial rock. This transmission electron microscope (TEM) study reports the first discovery of terrestrial silicate hollandite in a strongly shocked anorthosite from the central uplift of the Manicouagan impact crater, Canada.

Petrographic observations: Aside of the most frequent constituent plagioclase, the shocked anorthosite contains K-feldspar, garnet, titanite, scapolite, and orthopyroxene as accessory phases. Optical inspection reveals that plagioclase and K-feldspar are in most cases completely converted into diaplectic glass with perlitic fissures. In the immediate vicinity of garnet (i.e., a mineral with higher shock impedance), feldspars can partially remain crystalline. A peculiar phenomenon is, for example, the partial isotropization of twinned plagioclase. Whereas one set of polysynthetic twins remains crystalline, the other became completely amorphous upon shock compression. This observation could be explained as an effect of the shock direction but it needs to be further inspected. Garnet, titanite, and orthopyoxene are minerals of higher shock impedance and hence show less shock damage than feldspars. They exhibit a strong internal fragmentation but retain their crystalline state. Titanite develops also mechanical twins. Planar deformation features have been observed in scapolite.

Besides the shock damage of minerals, the "glassy" rock shows also traces of shock in form of several grayish to brownish shock veins, which pervade the rock in an irregular fashion. At the optical scale it is already obvious that the thin (< 100 µm) veins contain birefringent phases but an identification is impossible due to the small grain size.

TEM study: For phase identification, we therefore employed an analytical PHILIPS CM20 FEG-TEM, operating at 200 kV. Prior to TEM analysis, the sample was thinned to electron transparency by ion-beam bombardment at low acceleration voltage of 3 kV. TEM observations and electron diffraction experiments show that the veins are composed of polycrystalline aggregates of silicate hollandite with grain sizes ranging from a few nanometers up to 0.1 µm (Fig. 1). The grains have spherical to lath-like shapes and are commonly surrounded by an amorphous silicate matrix. As a consequence of the nanocrystalline nature of aggregates, one observes almost complete rings in electron diffraction patterns with interplanar spacings fully compatible with the hollandite structure. EDX measurements reveal that silicate hollandite has a feldspar composition ($Ab_{41}An_{58}Or_1$) equivalent to that of the maskelynite in the bulk anorthosite (Fig. 2).

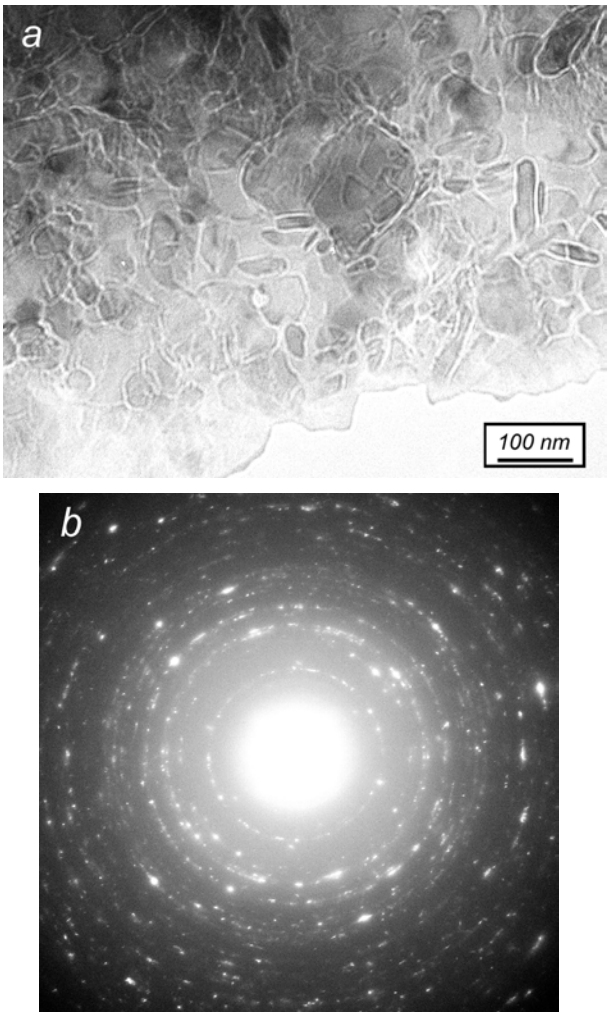

Fig. 1. (a) Bright-field TEM image and (b) corresponding selected area electron diffraction (SAED) pattern of a polycrystalline silicate hollandite aggregate from the Manicouagan impact structure, Canada.

Conclusions: We report here the first discovery of silicate hollandite in a terrestrial impact rock. Similar to heavily shocked meteorites, the silicate hollandite occurs in shock veins, i.e., in certain zones of the host rock where frictional movements led to localized melting [6]. The silicate hollandite crystallized from this high-pressure melt, as is evidenced by the small grain size and the embedding in an amorphous matrix. According to [6], the thickness of veins points to crystallization within a time frame of less than one millisecond. The isotropization of feldspars indicates that the host anorthosite has been shocked to pressures on the order of 35 to 40 GPa [7,8]. Silicate hollandite has however crystallized at lower pressures during the decompression phase since the stable assemblage at 35 to 40 GPa would be Ca-ferrite + stishovite [1].

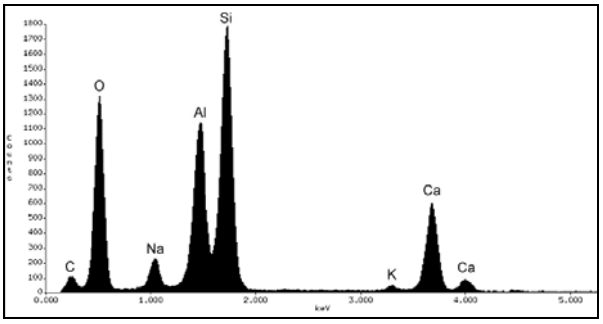

Fig. 2. Energy-dispersive X-ray spectrum of the polycrystalline silicate hollandite aggregate shown in fig. 1.

References: [1] Yagi A. et al. (1994) *Phys. Chem Min., 21*, 12-17. [2] Gillet P. et al. (2000) *Science, 287*, 1633-1636. [3] Tomioka N. et al. (2000) *Geophys. Res. Letters, 27*, 3997-4000. [4] Xie X. et al. (2001) *EJM, 13*, 1177-1190 [5] Langenhorst F. and Poirier J.-P. (2000) *EPSL, 176*, 259-265. [6] Langenhorst F. and Poirier J.-P. (2000) *EPSL, 184*, 37-55. [7] Ostertag R. (1983) *J. Geophys. Res., 88*, 364-376. [8] Langenhorst F. (1989) *Meteoritics, 24*, 291.

MAGNETIC, GRAVITY AND SEISMIC CONSTRAINTS ON THE NATURE OF THE WANAPITEI LAKE IMPACT CRATER. E. L'Heureux[1], H. Ugalde[2], B. Milkereit[2], N. Eyles[3], J. Boyce[4] and W. Morris[4],[1]Dept. of Physics, Univ. Toronto, 60 St. George, Toronto, Ontario, Canada, elizabeth.lheureux@utoronto.ca, [2]Dept. of Physics, Univ. Toronto, 60 St. George, Toronto, Ontario, Canada, [3]University of Toronto at Scarborough, Toronto, Canada, [4]School of Geography and Geology, McMaster Univ., 1280 Main street West, Hamilton, Canada

Introduction: The Wanapitei Lake impact crater (46°45'N, 80°45'W) is located in Northern Ontario, bounded on its West side by the deformed East rim of the 1.85 b.y. old Sudbury impact structure. The crater is believed to be of medium size (with a diameter of ~7.5 km) and lies entirely within the central, circular portion of the 9 km diameter Wanapitei Lake [1]. Because the crater lies underwater, there are few constraints on its actual size: its suggested diameter is based solely on one gravity survey. There are only few samples presenting shock metamorphic features in proximity of the lake, all of which come from glacial drift South of Wanapitei.

The regional setting of Lake Wanapitei presents a unique opportunity for the study of impact craters. Prominent diabase dikes extend for several kilometers across both the Sudbury structure and the lake, offering clear markers indicative of large tectonic or structural disruptions. For this study we used these dikes as a new method for delineating the crater's structure, as brecciation will have an effect on both densities and magnetic susceptibilities of target rocks, disrupting any linear anomalies produced by them. In addition, geophysical surveying over the crater is facilitated by the fact that it lies underwater, allowing for faster marine surveying.

Impact Indications: Dence and Popelar [1] presented topographic, geophysical and petrographic evidence to support the impact theory. Topographic evidence includes the shape and drainage pattern of the lake as well as an apparent concentric pattern of streams and smaller lakes within 5 km of Wanapitei. Although not thoroughly mapped, Dressler [2] observed a similar circular pattern in joints and fractures of the region. Shatter cones have been found on certain islands in the southern part of the lake as well as on shore, but cannot be unequivocally attributed to the Wanapitei structure.

The last published geophysical data from the lake dates back to 1972, when a gravity survey revealed a ~15 mgal low over the north-central, island free area of the lake. The data was corrected using water depth measurements from the Ontario Department of Lands and Forests, however bathymetry taken in 2002 has provided new and more precise depth estimates (Fig. 1).

More recent petrographic evidence comes from rock samples demonstrating shock metamorphic effects (quartzite fragments and the presence of glass) that have been found in glacial drift on the southern shores of the lake [1, 3, 4]. These include boulders of suevite and glassy breccia as well as samples of coesite [3]. Dressler [2] observed deformation lamellae in a few quartz grains at only three locations in the southwestern region of the lake.

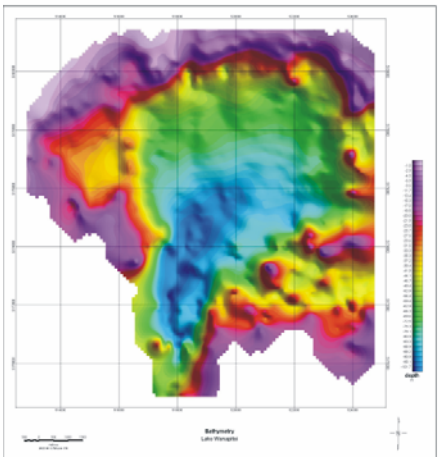

Figure 1: Bathymetry of Wanapitei Lake

Winzer et. al. [5] dated two samples of glacial drift and found them to be 37 ± 2 m.y. old, based on K/Ar dating. These dates were obtained on one glass vein and one whole-rock sample from glassy boulders.

Dence and Popelar [1] argued that the samples of glacial drift originated in the bottom of the lake, stating that the boulders are weakly compacted and disintegrate upon handling. They are also concentrated around the southern shores of the lake (in the Massey Bay area), said to be because of recent Pleistocene glaciation which has scoured the lake bottom and transported the boulders southward.

Target rocks are of the Huronian Gowganda and Mississagi formations (2.5 b.y.) and are intruded by Nipissing and younger diabase dikes (aged 1.2 b.y. [6]). Dence and Popelar [1] discovered boulders of glacial drift of the Mississagi and Nippissing formations.

Study Description: We present here the results of a survey to determine the exact dimensions and location of the Wanapitei crater, making use of the Sudbury swarm dikes as vertical markers. These 50-120 m wide Precambrian olivine diabase dikes trend North-

West throughout the Sudbury region and predate the proposed Wanapitei impact (Fig. 2). They exhibit a strong, linear total field magnetic anomaly (up to 1000 nT), suggesting they be used as prominent features in a survey to track possible disruptions in the local magnetic field. They are also more resistant to erosion than surrounding rocks, and were observed to outcrop in several places on both the East and West sides of the lake.

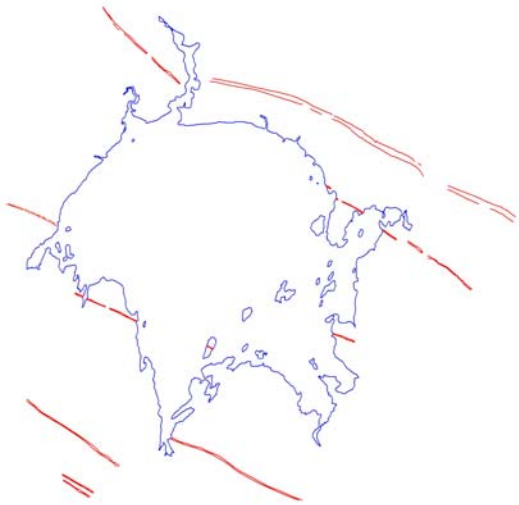

Figure 2: Wanapitei Lake and surrounding dikes. Extracted from Dressler [2].

Conclusions: A shallow total field magnetic survey was run in August 2002 and demonstrates a definite break in the linear dike anomalies (Fig. 3). It also indicates a circular low approximately 2.5 km wide, coinciding with the absence in dike anomaly and placed over the greatest depths of the lake (~110m). It is therefore not known whether the low can be absolutely attributed to an impact structure or whether it is due to the large water depths. This magnetic low does not correspond to the same dimensions as the gravity low. Data from a high frequency seismic survey will be used to estimate the amount of sediment infill in the lake basin and thus its effect on the magnetic and gravity signatures. It should also serve to track the dikes through the center of the lake.

Results thus far indicate that if the observed structure is due to a meteorite impact, it is at most a 3 to 4 km diameter simple crater. On the other hand, the bathymetric structure of the lake may also be suggestive of a more regional deformation, such as large scale faulting. A regional fault system has been suggested to run from ~49°N down to just above Lake Wanapitei, but no evidence was found to suggest its extension through the lake [7]. The new bathymetry presented here shows a linear scarp that runs North-South and defines the western edge of the southern half of the lake. This faulting could explain the disruption in dike signatures as well as the observed magnetic low, therefore discounting the impact theory. Large sedimentary deposits within the central basin of the lake further explain the gravity and magnetic lows. Indeed, river channels terminating in the lake contribute to deposition and it can be observed that the northern shore is overlain by several tens of meters of glacial deposits. Further investigation into the subsurface structure is needed to fully understand the formation observed under and around Lake Wanapitei.

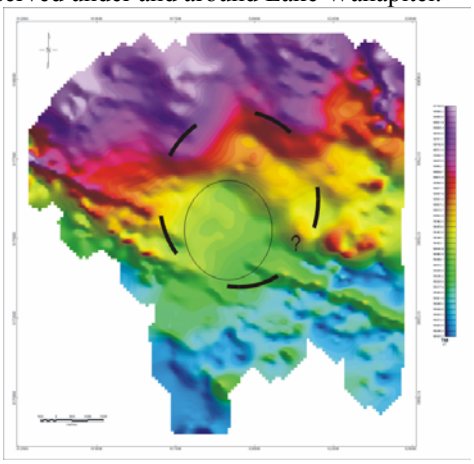

Figure 3: Total magnetic field map over Wanapitei Lake. Estimated maximum and minimum sizes for the impact crater are indicated.

References: [1] Dence, M.R. and Popelar, J. (1972), *Geol. Assoc. Can., Sp. Pap. 10,* p.117-124. [2] Dressler, B.O. (1982), *Ont. Geol. Surv. Rep. 213*, 131 pp. [3] Dence, R., Robertson, P.B. and Wirthlin, R.L. (1974), *Earth Plan. Sci. Lett., 22*, p. 118-122. [4] Grieve, R.A.F. and Ber, T.J. (1994), *Meteoritics*, *29*, p. 621-631. [5] Winzer, S.R., Lum, R.K.L. and Schuhmann, S. (1976), *Geochim. Cosmochim. Acta, 40*, p. 51-57.[6] Krogh, T.E., Corfu, F., Davis, D.W., Dunning, G.R., Heaman, L.M., Kamo, S.L., Machado, N., Greenhough, J.D. and Nakamura, E. (1987), *Geol. Assoc. Can., Sp. Paper 34,* pp. 147-152. [7]Buchan, K.L. and Ernst, R.E. (1994), *Can. J. Earth Sci. vol. 31*, p. 1197-1205.

AN ARRAY OF OFFSHORE IMPACT CRATERS ON MID-ORDOVICIAN BALTICA. Maurits Lindström, Department of Geology and Geochemistry, Stockholm University. S-106 91 Stockholm, Sweden (maurits.lindstrom@geo.su.se)

The purpose of this paper is to discuss paleodepths at five sites of offshore impact and relate them to the geological situation on the paleocontinent Baltica. The target in all cases consisted of Proterozoic crystalline rocks that were overlain by about 80-150 m thick Cambrian and Ordovician sediments. These sediments, which were in their turn covered by different depths of water, had well lithified limestone only in their uppermost 20-50 meters. Sands and clays, forming the lower part of the sediment cover, were to a large extent non-lithified. The impact structures vary in their mode of preservation, but all have a distinct morphologic crater excavated in the crystalline basement . This excavation is the only preserved part of the apparent crater in two of the cases. Its width, henceforth referred to by Ø, may be appreciably smaller than the transient crater that formed in water. The craters are, from east to west (Fig. 1), **Kärdla** [1] (about 455 Ma, Ø = 4 km), **Tvären** [2] (about 455 Ma, Ø = 2 km), **Hummeln** [3] (about 475 Ma, Ø = 1.2 km), **Granby** [4] (about 475 Ma, Ø = 2.5 km), and **Lockne** [5] (about 455 Ma, Ø = 7.5 km).

Hummeln and Granby are sub-circular, 200-400 m deep hollows bottoming in intensely brecciated crystalline bedrock. The only filling that is preserved in the case of Hummeln consists of slumped and brecciated, pre-impact sedimentary rocks. At Granby a filling of the same kind is completed upwards by post-impact sediments. Both craters are eroded, but Granby has the remains of a crystalline rim wall that projects through the post-impact sedimentary cover. This cover was stripped by erosion in the case of Hummeln. Neither of the two craters is explicable by anything but impact, but no shock metamorphosis has been found. Quartz with PDF occurs abundantly in connection with the other three craters. Hummeln and Tvären are dated by the youngest sediment occurring as clasts in the polymictic breccia within the crater, but at the other three there are marine sediments that formed before as well as after the impact that are biostratigraphically coeval.

No undoubted Middle Ordovician shorelines are preserved on Baltica, but voluminous oilshale interlayers in offshore carbonates south of the Gulf of Finland consist of freshwater algae [6] that must have come from a nearby land area. The only possible location of this land area is the north side of the Gulf (Fig. 1). **Kärdla** is situated on but gently sloping basement about 100 km off this shore. The paleodepth for the time of impact may be about 75 m. Kärdla differs from land impacts through the voluminous slumping of Cambrian sand and wet flow of ejecta and coarse debris of Ordovician limestone into the crater, following upon excavation and overwhelming much of the crystalline rim wall that was broken through completely in the south and northwest The crystalline basement rose at least some 160 m above its original level in the highest preserved parts of the wall. **Tvären** may have been less than 300 km from the land area in Finland. The probable paleodepth was over 150 m because filling was by resurge of the sea after excavation and was unimpeded by the rim wall. If it had been less, the rim wall would probably have prevented the massive introduction of water-carried resurge sediments, as the case was at Kärdla. The depth was probly not much over 200 m because shallow-water biota thrived on whatever remained of the rim wall during secular infill, and this rim wall would not have been higher than some 150 m by comparison with Kärdla.

Fig. 1. Localities referred to in the text. The west-east

width of the figure corresponds to 1400 km. The land to sea boundary along the Gulf of Finland is at the present the best available paleodepth constraint.

Hummeln and **Granby** formed during a major regression of the sea. They share with Kärdla the feature that resurge sediments are either missing or insignificant. Instead they became filled, like Kärdla, with slumped and brecciated sediments from the periphery. Crystalline ejecta are less important in this filling than at Kärdla. There are no indications of impact melt at Hummeln, which is the smaller of the two. In the case of Granby the necessary petrologic study is still wanting, but the geologic map [4] shows a rock otherwise

not occurring on the map-sheet, referred to as unspecified metavolcanic, that follows the crater periphery.

Lockne is excellently exposed at the present erosive front of the Caledonides and about 300-500 km west of the Finland shoreline. Paleodepth by modeling may have been about 700 m [7], which suggests downbending of the lithosphere toward the nascent Caledonides. Resurge of sea-water filled the crater excavated in the basement with clastics eroded from the surrounding cover rocks, as well as with ejecta clasts. No body of impact melt has been identified, but melt particles are abundant in the resurge arenites. There is no appreciably raised rim wall but instead, surrounding the western sectors of the morphologic crater there are extensive masses of ejected and overturned crystalline target rock that rest either on thin remains of sediment cover or on clean-stripped crystalline basement. Stripping is explained as an effect of the excavation of an extensive transient water-crater; emplacement of the crystalline ejecta masses occurred just before the collapse of this water crater.

[1] Puura V. and Suuroja K. (1992) *Tectonophys., 216,* 143-156. [2] Lindström M. et al. (1994) *Geol. Mag., 131,* 91-103. [3] Lindström M. (1999) *GFF, 121,* 243-252. [4] Wikman H. et al. (1982) *Sveriges Geol. Undersökn., Ser. Af, 120,* 1-112. [5] Lindström M. and Sturkell E.F.F. (1992) *Tectonophys., 216,* 169-185. Lindström M. et al. (1996) *GFF, 118,* 193-206. [6] Guy-Ohlson D. (1992) *Rev. Palaeobotan. Palynol., 71,* 1-15. [7] Ormö J. et al. (2001) *Meteoritics & Planet. Sci., 36,* A154.

ON THE DECOUPLING OF MICROTEKTITES FROM THE EJECTA PLUME. R.D.Lorenz, Lunar and Planetary Lab, Department of Planetary Sciences, University of Arizona, Tucson, AZ 85721-0092. (rlorenz@lpl.arizona.edu)

Introduction: Cratering on planetary bodies with atmospheres entails significant interaction of ejecta with the atmosphere. In addition to the obvious (to remote sensing) proximal effects associated with blast and wake scouring and the restraint of the ejecta curtain to form lobate blankets rather than rays, the atmosphere as a whole controls the expansion of the impact fireball and the subsequent release of fine particulates entrained in, or condensing from, it. The details of this process must control the distribution of microtektites which are distributed on exoatmospheric (i.e. ballistic) trajectories after release. Here I aim to connect the distribution of launch parameters (velocity, angle, altitude) with the particle size : this association should shed light on the plume expansion and particle launch process.

Constraints: There are 3 principal lines of evidence which allow us to place constraints on the ejecta launch parameters. These are :

1. The thickness of microspherule and ejecta layers from a handful of terrestrial impact craters (e.g. Chicxulub; Bosumtwi; the as-yet source crater of the Australasian microtektites [1] and the recently-discovered UK ejecta layer, probably from Manicouagan [2]) As yet there is only limited data on the variation of size with distance from the source. Relationships between ejecta thickness and distance exist in the literature (e.g. see summary in [3]) and provide lower limits on the required launch velocity. However, it is typically assumed for these investigations that the particles are launched from a point source.

2. The shape and estimated thickness of dark parabolic ejecta deposits of fresh craters on Venus, observed in Magellan radar imagery, e.g. [4]. The shape of these deposits, where exoatmospherically-dispersed ejecta is winnowed in the zonal wind field, can be fit by models indicating the amount and size of ejecta particles as a function of distance from the source crater [4,5].

3. The expansion of the fireball associated with impacts of comet Shoemaker-Levy 9 with Jupiter, as observed by the Hubble Space Telescope.

Method: The problem does not appear to lend itself to analytic solution. The parameter space is therefore being explored numerically – similar approaches have been used to study volcanic ejecta dispersal on Mars [6] and eruption plumes on Io [7]. Each bin in the impact ejecta size distribution can be associated with an angle and speed distribution. It is assumed that ejecta is launched in a radially symmetric fashion (i.e. that the azimuth distribution of the launch velocity is flat).

The particles are launched at some altitude, travel near-ballistically until they reach some altitude where they are rapidly decelerated and fall at terminal velocity. During their descent to the ground they are displaced horizontally by a wind field.

Since the distance over which sub-mm grains or drops can travel through the atmosphere is extremely small (compared with the >100km dispersal distances associated with Venus dark parabolar, for example) the grains must be launched at very high altitude. At such altitudes the plume must have expanded considerably beyond the size of the crater itself. But some obvious questions are whether the size-distance relationship inferred from these parabolae is consistent with simple drag in an adiabatically expanding plume, or whether the expansion and release must be more complex. Similarly, are the particles launched isotropically, or are they collimated in elevation ?.

Prospective: The modeling work identified here is presently underway – preliminary results will be available at the meeting. New data may help shed light on this problem : in particular

1) identification and recovery of microtektites from other terrestrial craters, in particular if size variation with distance can be determined
2) further analysis of Magellan radar data, to interpret not only the shape of the parabolic features but also the radiometric effect of the ejecta layer on the emissivity and backscatter, which must constrain the thickness and particle size of the layer. [8]

It may be that information on the wind field as a function of latitude can be recovered from the dispacements of falling ejecta.

3) observations of the surface of Saturn's moon Titan which has a thick atmosphere [9]. The large scale height of this atmosphere makes it perhaps unlikely that parabolic ejecta features form as on Venus, but the characteris-

tics of wind streaks downwind of craters can probably be interpreted as dumping of ejecta from the fireball. (This is not the case on energetic Mars, where most wind streaks appear to be post-cratering Aeolian features.)

It is worth making the additional remark that plume interactions have been considered in the so-called 'hyper-ballistic' dispersal of Copernican ejecta on the moon [10].

References: [1] Glass, B. P. and J. E. Pizzuto, Geographic Variation in Australian Microtektite Concentra-tions: Implications concerning the location and size of the source crater Journal of Geophysical Research, 99, 19075-19081 (1994) [2] G. Walkden, J. Parker and S. Kelley, A Late Triassic Impact Ejecta Layer in Southwestern Britain, Science, 298, 2185-2188 (2002) [3] R. D. Lorenz, Microtektites on Mars : Texture and Volume of Distal Impact Ejecta Deposits, Icarus, 144, 353-366 (2000) [4] Vervack, R. J. Jr., and H. J.Melosh, Wind Interaction with Falling Ejecta: Origin of the Parabolic Features on Venus, Geophysics Research Letters, 19, 525-528 (1992) [5] C. J. Schaller and H. J. Melosh, Venusian Ejecta Parabolas: Comparing Theory with Observations, Icarus, 131, 123-137 (1998) [6] Fagents, S. A. and L. Wilson, Numerical Modeling of Ejecta Dispersal from Transient Volcanic Explosions on Mars, Icarus, 123, 284-295 (1996) [7] L. S. Glaze and S. M. Baloga, Stochastic-ballistic Eruption Plumes on Io, J. Geophysical Research, 105, 17,579-17,588 (2000) [8] Campbell, B. A. et al., Magellan Observations of extended impace crater related features on the surface of Venus, J. Geophys. Res., 97, 16,249-16,278 (1992) [9] R. D. Lorenz, 'Impacts and Cratering on Titan - a pre-Cassini View' Planetary and Space Science, vol. 45, 1009-1019 (1997) [10] Rehfuss, D. E., D. Michael, J. C. Anselmo, N. K. Kincheloe and S. A. Wolfe, Hyper-Ballistic Transport Models of Copernican Ejecta, Proceedings 8th LPSC, 3375-3388, 1977

ORIGIN OF EPIDOTE FROM THE IMPACT MELT OF THE CHICXULUB CRATER, MÉXICO. E. Lounejeva[1] , M.Elias-Herrera[1], F.Ortega-Gutiérrez[1], and E. Cedillo-Pardo[2], [1]Instituto de Geología, Universidad Nacional Autónoma de México, (e-mail: elenal@servidor.unam.mx, elias@servidor.unam.mx, fortega@servidor.unam.mx) [2] Instituto Mexicano del Petroleo (cedillo@www.imp.mx).

Introduction: Epidote is a typical mineral from low-grade metamorphic rocks, contact metasomatism and hydrothermal processes. Igneous epidote originally identified in deep-seated granitic plutons [1-5], has also been reported with growing frequency in shallow intrusions [6, for example]. Normally it forms euhedral to anhedral crystals and appears in association with hornblende and biotite.

There are different criteria for distinguishing the igneous vs subsolidus origin of epidote: the euhedral shape, zonation with allanite-rich core [2] and, in general, Sr and REE enrichment, and the magmatic oxygen isotopes relationship ($\delta^{18}O$ >4.2) [5]. Other criteria include textural relationships, mineralogical paragenesis, and trace element geochemistry of other accessory minerals such as apatite, for example [3].

Experimental results on epidote stability in granitic melts [8,9] estimulated its use as an indicator of high pressure-temperature emplacement [1,7]. Later it was shown [10] that an increase of oxygen fugacity extends the field of stability of epidote to lower pressures (up to 2 kbars) and higher temperatures (>790°C). The studies of the dissolution kinetics of epidote [10] have shown that the quick up ward emplacement contributes to preserve the magmatic epidote.

In this work we report the presence of accessory epidote at the impact melt from the Chicxulub crater. Based on petrographic observations, we infer an igneous origin for the epidote.

Samples: The petrographic study was carried out on ten thin sections of sample C1N10 (interval 1393-1394 m) from the Chicxulub- 1 borehole situated approximately 20 km from the center of the impact structure.

Results and discussion: Petrography of the holocrystalline melt shows that it is composed mainly of anhydrous primary phases such as plagioclase, augite, quartz, alkalic feldspar, and Fe-Ti oxides. We infer that the only water-containing primary phase is the accessory epidote in crystals with cross section up to 400 μm across. Secondary alteration includes replacement of primary phases by epidote, albite, chlorite, hematite, titanite, and the formation of authigenic pyrite, chalcopyrite, bornite and calcite.

The petrographic criteria we used to infer the origin of accessory epidote are as follows. The accesory epidote inferred to be of igneous origin is distinguished from the secondary one by its euhedral or subhedral shape, high relief and normal 1st order red-blue birefringence. Zonation as an evidence of growing from liquidus was observed in some crystals. The euhedral epidote is occasionally associated with tabular unzoned anorthite crystals surrounded by plagioclase ($An_{>70}$) and quartz in myrmekite-like texture.

The composition of euhedral as well as of anhedral (secondary) epidote is given in Table 1. It should be noted that its clinozoisite and the pistacite ($Fe_2O_3/(Fe_2O_3+Al_2O_3)$) components are lower and higher than those corresponding to the secondary epidote, respectively. We observed that in one analyzed crystal the border is more rich in iron than the core. It could be a consequence of pressure decrease in agreement to the experimental results [10], in wich epidote obtained at lower pressures is richer in iron (Ps_{21} at 6.5 kbar) than the epidote at high pressure (Ps_8 at 18 kbar).

The presence of primary epidote has some implications for the crystallization history of the melts. Geological setting and petrology of Chicxulub melts rule out the high static pressure scenario. Water activity is difficult to estimate in high-temperature rocks, but factors such as water saturation over 12% and high fO_2 seem to be compatible with the initial stage of crystallization of the impact melts.

Conclusions: We infer the presence of primary igneous epidote in Chicxulub melt rocks. More detailed analyses of trace elements and oxygen isotopes underway will permit to confirm or discard tha magmatic origin of that epidote.

Table 1. Energy-Dispersive Spectrometry analyses of epidote from the Chicxulub melt rock.

	Euhedral (primary)	Anhedral (secondary)
Oxide	**Weight %**	**Weight %**
SiO2	42.5 ± 3.4	37.7 ± 3.0
TiO2	0.4 ± 0.2	0.4 ± 0.4
Al2O3	24.2 ± 1.4	22.1 ± 2.2
Fe2O3 (total iron)	10.2 ± 1.8	14.3 ± 2.8
MnO	0.3 ± 0.3	0.5 ± 0.4
MgO	0.6 ± 0.4	0.3 ± 0.2
CaO	21.3 ± 2.2	24.2 ± 2.3
Na2O	0.4 ± 0.2	0.3 ± 0.2
K2O	0.1 ± 0.0	0.1 ± 0.0
Total	99.9 ± 0.2	99.77 ± 0.2
Ps (pistacite mol.%)	30 ± 5	37 ± 2
Al/Fe (clinozoisite component)	3.4 ± 0.7	2.21 ± 0.61

References: [1] Zen, E-an, and Hammarstrom, M. (1984) *Geology, 12,* 515-518. [2] Dawes, R.L. and Evans, B.W. (1991) *Bulletin of Geological Society of America, 103,* 1017-1031. [3] Smirnov, V.N. and Zin´kova, Ye.A.(1995)

Transitions (Doklady) of the URSS Academy of Earth Sciences, Sec.329 A, (199-504), 105-107. [4] Foritz, I, et al. (1995) *USGS, 1995,* 53-55. [5] Keane, S.D. and Morrison, J. (1997) *Contribution to the Mineralogy and Petrology, 126,* 265-274. [6] Sial, A.N. et al. (1999) *Lithos, 46,* 367-392. [7] Christofides et al. (1990) *European Journal of Mineralogy, 2*, 79-87. [8] Naney, M.T. (1983) *American Journal of Science, 283,* 993-1033. [9] Schmidt, M.W. and Thompson, A.B. (1996) *American Mineralogist, 81,* 462-474. [10] Brandon, A.D. et al. (1996) *Science, 271,* 1845-1848.

Acknowledgments: We sincerely thank Dra. M. A. Reyes Salas for help with EDX microprobe analyses.

ORIGINAL DIAMETER AND DEPTH OF EROSION OF THE POPIGAI IMPACT CRATER, RUSSIA.
V.L. Masaitis, M.S. Mashchak and M.V. Naumov, Karpinsky Geological Institute, 199106 Sredny prospekt 74, St.-Petersburg, Russia, vicmas@vsegei.sp.ru

Veritable evaluations of diameters of large terrestrial impact structures remain questionnable because most of the craters are essentially modified by erosion or buried beneath younger sediments. In contrary, about 35-Ma old Popigai impact structure (Northern Siberia) represents the well-preserved large impact structure. Its preservation and geological and geophysical studies carried out in its area allow precisely estimating its original diameter and depth of erosion.

The Popigai crater formed in the two-layered target composed of Archean and Lower Proterozoic crystalline rocks overlain by 1.5 km sequence of Upper Proterozoic, Lower and Upper Paleozoic and Mesozoic sediments. The crater fill of about 2 km thick consists of allogenic breccias and diamond-bearing impactites – tagamites (impact melt rocks) and suevites. The Neogenic and Quaternary gravels and sands overlay the central part of the crater depression. Main morphostructural characteristics of the crater are (1) a circular center depression (D=40 km); (2) a peak ring (D=45 km); (3) an annular trough (outer diameter D=72 km); (4) an outer flat terrace, where disturbed target rocks and relics of allogenic breccia can be observed (D=100 km). Small remnants of the ejected allogenic breccia are traced up to 75 km from the crater center mostly to the north from the structure.

The size of the Popigai impact structure was evaluated on the ground of measurements of the topographic and structural features, and also from analyses of geophysical data. The moderate erosion gives the best opportunity for these evaluations in the northern and northeastern crater sectors.

The rim-to-rim diameter can be estimated due to preservation of the remnants of the original crater topography. They are represented by the discontinuous topographical highs in the outer edge of the terrace, where the impact dislocations attenuate. Probably, the original structural rim was discontinuous too. The former crater rim was complex, and composed of uplifted target rocks (socle or bedrock rim) upon which allogenic breccia was piled on (embankment rim). The remnants of this complex rim form hills, made of thrust-faulted Cambrian carbonate rocks, and located in the northern and northeastern sectors of the structure. The absolute heights of the hills (they form the arcuate chain parallel to the edge of the crater depression) reach up to 250 m, and in places to 350 m. The absolute height of local relief in the vicinity of these hills is approximately 150-250 m. Small fragments of disintegrated ejected allogenic material can be found here and there at the foots of the hills and on its slopes. It means that the structural uplift of the target rocks in the rim zone was about of 100-200 m. Meanwhile the apparent crater bottom in the central depression, where the allogenic breccias (including microbreccia or coptoclastites) and minor suevites occur, has an altitude of 30-80 m.

The chain of the hills is traced up to 60-70 km from northwest to southeast, and their summits are located at a distance of about 50 km from the crater center. Small patches of ejected allogenic breccia were mapped in the area located northeast and east of these hills.

The similar features are observed in the northwestern sector. Isolated hills composed of uplifted blocks of Upper Proterozoic sandstones are about of 250 m high. The summits of the hills are located at a distance 46-48 km from the crater center, but the erosion is deeper here. The remnants of the ejecta blanket of blocky allogenic breccia are dispersed on the hill flanks.

The structural construction (based on the mapping and geophysical data, and in part on drillcore study) showed that the contour line +150 m of the surface of the true crater floor, which is made of disturbed and slightly displaced target rocks, may be considered as the outer border of the flat bedrock terrace outlined by remnants of the structural crater rim. In general, the radii of this contour line measured in the northeastern and eastern sectors is about 50 km.

The gravimetric map shows (especially in the northwestern sector) that the axis of the arched positive anomaly that coincides with arched underground uplift of the crystalline basement is located at a distance of about 49-51 km from the crater center. This positive anomaly coincides on the whole with the topographic highs in this sector as well.

All these data combined show that original rim-to-rim diameter of the Popigai crater (e.g. diameter of the final crater formed at the end of the early modification stage) may be firmly estimated as 100 km.

Erosion and accumulation of recent deposits accompanied by some tectonic movements modified the initial morphology of the impact crater during last 35 Ma. The piled-on crater rim was destroyed, as well as the main part of the ejecta blanket outside the crater, and as well upper horizons of the crater fill. The finds

of impact diamonds dispersed in some riverbeds far from the crater show that ejecta blanket originally covered the surface at a distance of about 2R or more from the crater center and later was washed out almost completely.

The original rim height of the Popigai crater can be evaluated according to the diameter/rim height ratio of lunar craters, also taking into account the difference of acceleration due to gravity, and presence of atmosphere. The estimated average original height of the complex crater rim may be of about 200 m, but probably it was not the same all around the crater. The piled-on allogenic breccia, including microbreccia (or coptoclastites) and suevites composing the rim has the total thickness up to 200-300 m. It is possible, that the crest of the former original rim was slightly displaced outward from the crater center, and rim-to-rim original diameter was slightly larger than 100 km.

Special study of the recent history of the crater relief showed that it subjected to several cycles of denudation and accumulation during the Neogene and the Quarter. Inferred from geological data, the sharp variations of the depth of denudation within the impact crater are proposed due to uneven block displacements during the late modification stage. The maximal depth of erosion occurs in the rim area, where all ejected material and partly structural rim were washed out. This depth is evaluated as much as 300-500 m in the southwestern sector, and about of 200-250 m in the northwestern sector. The denudation was two times less significant in the inner depression of the crater. The total volume of the washed out breccias and suevites (taking into account the rate of erosion during recent geological periods) was about of 1200 km^3. The main part of this lost volume was composed of loose allogenic breccia (coptoclastite) occurred in the uppermost layer of the crater fill. As a whole, about of 20% of impact rocks were eroded.

The defined principal data of the original crater morphology and depth of erosion give an opportunity for the more precise reconstruction of some other initial parameters of the Popigai impact structure.

NUMERICAL MODELING OF LARGE IMPACTS. H. J. Melosh, Lunar and Planetary Lab (University of Arizona, Tucson AZ 85721) jmelosh@lpl.arizona.edu.

Meteorite impacts can be studied by computer simulation: Large meteorite impacts are among those phenomena that are either too large or too dangerous to study experimentally. Although impacts have affected the formation and surfaces of nearly every body in the solar system, we are limited to observing the results of past events. Investigation of impact processes is thus divided into observational studies of the traces of past impacts, small-scale analogue laboratory experiments and, most recently, detailed computer modeling. Computer models offer the possibility of studying craters at all scales, provided we completely understand the physics of the process and possess enough computer power to simulate the features of interest [1].

But computer models cannot do everything! One of the most common disappointments of geologists not familiar with modeling is that computer simulations cannot answer all questions we might like to ask. Numerical simulations suffer two major shortcomings: One is that they cannot treat processes that are not included in the computer code. Thus, no computer code presently treats the chemical or isotopic interactions that occur during an impact. This does not mean that such processes are untreatable, just that the appropriate codes that embody the correct physics must be created. In some cases the physics is poorly known and research must be done to improve the basic foundations. The second shortcoming stems from resolution in both space and time. All digital computer simulations depend on dissecting time and space into discrete blocks. The number of such blocks is limited by the amount of time and physical memory available for the computation. These limits can be easily exceeded by even an apparently modest computation. Thus, if an investigator wants to know about the dynamics of meter-size ejecta blocks in a 10 km diameter impact crater, he or she may discover that the required resolution far exceeds the capacity of any existing computer (a 3-D computation must include at least 10^12 computational cells!). Models to "predict" the effects of the impacts of Shoemaker/Levy 9 fragments with Jupiter [2] were still running at the time of the impacts, more than a year after the comet was discovered! These limitations can be surmounted both by faster computers with more memory as well as by better solution algorithms, such as the recent adoption of SPH codes when both hydrodynamics and self-gravity are important in a simulation [3].

A second, subtler, problem that arises from spatial discretization is that the material in any given cell is treated as if it were homogeneous. Thus, although the shock wave may break the rock into many blocks along discrete faults, the hydrocode knows nothing of this and instead computes the strain as if it were homogeneous. If properly understood, this is not a problem, because the modeler knows not to attribute physical reality to features below the scale of the mesh. Sometimes, accessory computations can fill in the details and permit estimates of the size and character of features not modeled at the scale practical in the computation. However, observers have been misled in the past by too-literal reliance on the output of numerical models and it is important to recognize this limitation. As an example, Figure 1 illustrates the difference between homogeneous strain and heterogeneous strain. The total strain is the same in both cases, and a numerical model with a cell size of several 100 m would not be able to distinguish the two, but a field geologist working at the scale of an outcrop certainly would notice the difference!

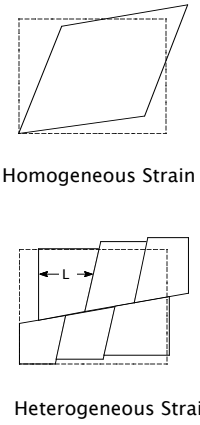

Figure 1. Homogeneous and heterogeneous strain can be readily distinguished in the field, but are not so clearly differentiated in hydrocode calculations. Common sense in interpreting the output of hydrocodes is essential!

Before beginning any computer simulation it is important to ask whether the numerical computation is capable of answering the desired question. Are all of the relevant processes included in the code to be used? Can the problem be solved in reasonable time on the available hardware? Too often the answer is "no" and the potential modeler must look elsewhere for enlightenment. But there **are** plenty of open questions that are still ripe for computer solutions.

The three pillars of impact simulation: The physics needed to simulate large meteorite impacts lies squarely in the classical domain. The size scale is so large that quantum effects are not important (although quantum mechanics does determine the thermodynamic equation of state) and the velocities are well below the speed of light, so classical Newtonian mechanics, supplemented by classical thermodynamics, provides an adequate framework for modeling impacts. In addition, it has become clear that successful simulation of real impact craters often requires a detailed understanding of the response of real rocks to stress and heat.

Of these three supporting pillars, Newtonian mechanics is probably the least troublesome. All modern "hydrocodes" (a now obsolete term that reflects the historical development of computer codes that, at first, did not contain material strength) incorporate the standard F = ma foundation of mechanics, although this is often obscured by an impressive amount of bookkeeping to keep track of all the pieces. All codes incorporate some form of gravitational acceleration, although only a few employ self-gravitation (only important in planet-scale impacts).

The next supporting pillar is thermodynamics, through the equation of state [4]. The equation of state for impact modeling is a little peculiar: Instead of the conventional thermodynamic relation relating pressure P to density ρ and temperature T, $P(\rho,T)$, hydrocodes require a relation between P, ρ and internal energy E. Equations of state for metals have been vigorously pursued by squadrons of physicists since the end of WWII, mainly to support the design and testing of nuclear weapons. However, few good equations of state exist for geologic materials, such as rock or ice. More research is needed to create these important relations.

Finally, in the late stages of an impact event material strength becomes important. Very little work has been done on good strength models for rock [5]. Porosity is also now recognized to play a key role for some impacts, especially on asteroids, which recent research has shown might be as much as 50% porous. Impact crater collapse and the morphology of large craters are controlled by strength, and observations suggest that a poorly understood mechanism must operate to greatly degrade the strength of rocks surrounding an impact site shortly after an impact event [6].

What next? Our ability to numerically simulate impact events is currently being taxed by a number of difficult problems. We are concerned about the possibility of impacts causing future extinctions, as they did at the K/T boundary. Two and three-dimensional models have already been used to estimate the mass and type of environmentally active gases released by the impact [7], but the ultimate effects of these gases on climate is still largely unknown. Chemical reactions of material in hot vapor plumes may be important for both environmental effects as well as explaining the observed oxidation state and isotopic fractions observed in the ejecta. Several new craters with unusual morphologies such as the Silverpit crater in the North Sea [8] and the Chesapeake Bay crater [9] challenge our understanding of the response of the Earth's surface to large impacts. Crater morphologies on Europa [10] may be indicating the thickness of the ice shell beneath the surface, but we must understand the cratering process better before we can cite a numerical value for the thickness. An active question is whether damaging tsunami result from relatively small impacts in the Earth's ocean. Solving this problem requires a full understanding of interactions near the surface and the physics of wave breaking, a new challenge to existing computer codes.

We currently have a list of urgent needs for making our simulations more realistic. Much work is needed in the near term on equations of state and constitutive models for geologic materials. Nevertheless, numerical modeling of impact processes has made important contributions to our understanding of impacts in the past and will surely continue to do so in the future.

References:

[1] Anderson, C.E. (1987) *Int. J. Impact Engineering* **5**, 33.
[2] Zahnle, K. & Mac Low, M.-M. (1994) *Icarus* **108**, 1.
[3] Benz, W. in *Numerical Modeling of Nonlinear Stellar Pulsation: Problems and Prospects* (eds. Buchler, J.R.) 269 (Kluwer Academic, Dortrecht, 1990).
[4] Melosh, H.J. *Impact Cratering: A Geologic Process* 1-245 (Oxford University Press, New York, 1989).
[5] Ivanov, B.A., Deniem, D. & Neukum, G. (1997) *Int. J. Impact Eng.* **20**, 411.
[6] Melosh, H.J. & Ivanov, B.A. (1999) *Ann. Rev. Earth Planet. Sci.* **27**, 385.
[7] Pierazzo, E., Kring, D.A. & Melosh, H.J. (1998) *J. Geophys. Res.* **103**, 28607.
[8] Stewart, S.A. & Allen, P.J. (2002) *Nature* **418**, 520.
[9] Poag, C.W. (1997) *Sed. Geol.* **108**, 45.
[10] Turtle, E.P. & Pierazzo, E. (2001) *Science* **294**, 1326.

Another Look at the Geophysical Signature of Large Terrestrial Impact Structures. B. Milkereit[1], [1]University of Toronto, Dept. of Physics, 60 St. George St., Toronto, Canada, M5S 1A7, bm@physics.utoronto.ca

Introduction: Most terrestrial impact craters exhibit geophysical signatures [1]. Recently, integration of results from seismic surveys, potential field studies, remote sensing, exploration drilling and numerical modelling of impact processes constrain the size and shape of transient craters and provide images of impact basin morphology. Common features of geophysical studies across the Vredefort (South Africa - diameter: 300 km; age: 2006 Ma), Sudbury (Canada - 250 km; 1850 Ma), Chicxulub (Mexico - 180 km; 65 Ma), Ries (Germany - 24 km; 15 Ma), and Bosumtwi (Ghana - 10 km; 1 Ma) structures are reflective target stratigraphy, quiet post-impact sedimentation, and prominent magnetic anomalies. The reflective target stratigraphy provides some information about the size of the transient crater and capture the footprint of crater collapse such as broad terraces, fault offsets and slumped blocks. The quiet post-impact sedimentation follows the redistribution of ejecta by high-energy wave action or crater wall slumping.

Magnetic Anomalies: Prominent magnetic anomalies of large impact craters are attributed to remanent magnetization as thermal effects induce extremly high Q-values. Magnetization of melt, breccias and footwall complex are related to the thermal evolution of large impact craters: from a single heat pulse to long-lived hydrothermal processes and associated alterations (and mineral deposits?) in the footwall and hanging wall.

Integration of Geophysical Data from the Chicxulub Structure: Based on seismic, magnetic, gravity and borehole geophysical data a 3D structural model of the Chicxulub crater has been proposed [2]. In a first step the 3D thickness of the Tertiary fill was reconstructed from reflection seismic profiles and borehole data. removing this infill results in a basin of 140-160 km diameter and 1-1.5 km depth with a central plateau of 90 km diameter and ~200m height surrounded by a depression (Fig. 1). The basin paleotopography has a rather smooth appearance compared to intact craters of similar size on other planetary bodies. This smoothness may be an indication of erosional processes by water wave actions immediately after the impact on the shelf area. Modelling the gravity signature of the 3D Tertiary infill results in too small amplitudes compared to the pronounced regional Bouguer gravity anomaly of the Chicxulub structure. The 3D sub-Tertiary structure was modelled on the basis of seismic, borehole and gravity data and consists of a central uplift of 20 km radius surrounded by a ring of megabreccias out to a radius of 35 km; a region of slumped blocks follows up to a radius of 70 km. The central zone of intermediate and short wavelengths of relatively high amplitude magnetic anomalies with a diameter of 90 km is shown in Figure 2. The magnetic signature coincides with the 90 km central plateau of the paleobasin and shows some important deviations from radial symmetry. The diameter of the paleotopographic basin of about 150 km supports estimates of a total crater diameter and the volume of the central melt body [3]

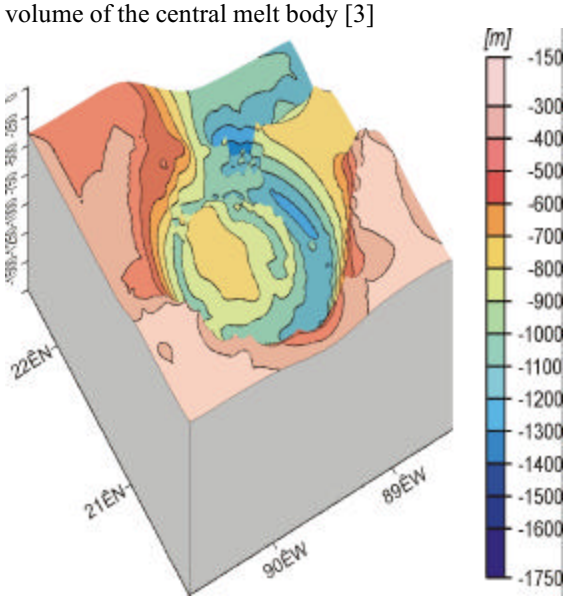

Fig. 1. Reconstruction of the palaeotopography of the Chicxulub crater from modeling of the thickness of the Tertiary infill based on seismic and borehole data. Perspective view from SW, 100x vertical exaggeration [2].

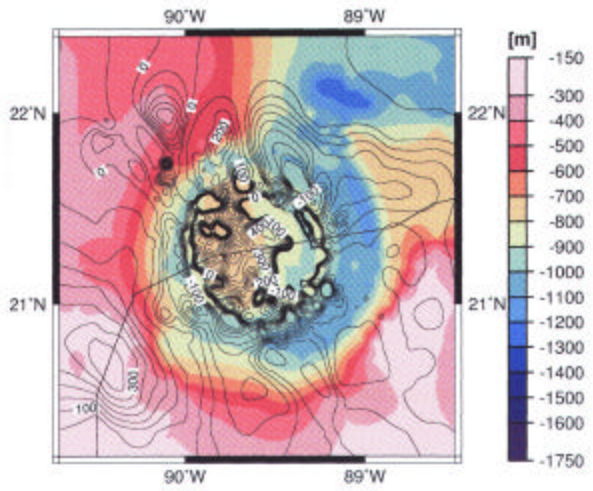

Fig. 2. The areal palaeotopographic map is combined with the magnetic anomalies (RTP) given in nT [4]. The area of the short wavelengths anomalies coincides well with the broad central plateau of the crater [2].

Summary: Understanding the nature and extent of excavation, brecciation, melt generation, slumping, lteration and late adjustments is esseantial in determining both, the energy release of the impact event and original shape and evolution of large impact craters. At present, geophysical determination of lithologies in deep craters remains problematic. Only the magnetic data seem to give indications of lithological control, although the physical mechanism (such as cooling of melts and breccias and/or post-impact hydrothermal alteration) need to be studies in more detail.

References: [1] Pilkington, M. and Grieve, R.A.F. (1992) Reviews of Geophysics, 30, 161-181 [2] Ebbing, J., Janle, P., Koulouris, J. and Milkereit, B. (2001) Planetary and Space Science, *49,* 599-609. [3] Kring, J., (1995) JGR, 100, 16979-16986 [4] Pilkington, M., Hildebrand, A.R. and Ortiz-Aleman, C. (1994) JGR, *99,* 13147–13162.

IMPACT DRILLED SAMPLES OF BURIED CRATER STRUCTURE AT TAKAMATSU-KAGAWA DISTRICT IN JAPAN. Y. Miura, N.Koga and A.Nakamura, Institute of Earth & Planetary Sciences, Faculty of Science, Yamaguchi University, Yoshida 1677-1, Yamaguchi , Yamaguchi, 753-8512, Japan. E-mail: yasmi-ura@yamaguchi-u.ac.jp

Introduction: Surface shocked materials lifted from crater bottom with later andesitic intrusion along cracks are reported by previous papers at Takamatsu-Kagawa district from Busshozan-Cho, Takamatsu-City to Kagawa-cho, Kagawa Prefecture, Shikoku Islands, Japan [1-3]. Drilled samples to 1,750m in depth are collected every 10m intervals as slice grains are studied by separated preliminary reports [4-8]. Purpose of the present paper is to make drilled profile and to elucidate shocked materials of quartz and Fe-Ni particles from buried crater which is probably related with formation of Japanese islands and Sea of Japan in Miocene Tertiary.

Drilled Samples: Borehole project of 1,750m in depth has been carried out at the Hotel Kansui (with courtesy of manager Mr.T.Oka) of north inside within buried crater of Takamatsu-Kagawa district to make hot spa project, where there is no mountain of andesite intrusion with hydrothermal veins. Deep drilled samples stored in Y.Miura Laboratory of Yamaguchi University up to 1,750m indicate that there are many layers of flow-in rocks and sediments from outside which are completely different with volcanic intrusion district of "the Goshikidai drilled samples" from 20km West-North of Takamatsu-Kagawa district in the same Kagawa Prefecture. Drilled samples up to 1,750m in depth have been checked as follows (Fig.1):

1) Layer of 0m to 170m:Complete buried crater structure was formed by the Alluvium sediment for 45m and conglomerate and clay of the Mitoyo group layer with 125m in thickness, which was formed in the water (sea or lake) sediments.

2) Crater sediments I (upper part) of the crater (170m to 450m) are flow-in sediments (of "round" granite of basement rock, andesite as intrusion and crystalline minerals from these rocks) from outside the crater for 280m in thickness. This indicates typical impact cratering event to the sedimentation process (not large type of volcanic event) at the later stage during or after filled event to form the buried crater.

3) Crater sediment II (lower part) of melt breccias brownish and black) for 675m in thickness(450m to 1,125m), which we can find only Fe-Ni-bearing grains (Fig.2) and spherules, together with shocked quartz grains in melted rocks.

4) Basement of granitic rock is found with recrystallized texture of quartz and feldspar from 1,125m to 1,750m in depth (i.e. 625m in thickness). There are a few percent of basaltic rock type in the drilled samples which indicate inrusion along cracks at later volcanic event during volcanic Goshikidai formation. However there no large volcanic rocks at granitic basements rocks of the buried crater.

Fe-Ni-Co grains: Fe-Ni rich grains (ca.10μm in size) are found at the crater sedimenst I of 230m and 420m, and the crater sediments II of 610m, 930m, 950m, 960m, 980m, 1,080m in depth (Fig.2). Spherules of polyhedral shapes (ca.50μm in size) are found at samples of 930m in depth. These Fe-Ni rich grains indicates that these Fe-Ni-Co rich grains are formed during mixture of Fe-Ni-Co grains from meteoritic impacts.

Shocked quartz: Shocked quartz of PDFs texture can be found at surface lifted from crater bottom and drilled crater sediments II (450m to 1,125m) of 460m, 690m , 960m and 1,120m in depth (Fig.2). This indicates that these shocked quartz minerals are formed at event of the sediment II as impact breccias. The main reason why we cannot find many shocked quartz minerals at this district is that a) basement rock of Rhyoke granite is so hard to make shocked feature (though it was crushed during the Koshikidai intrusion from North-West direction), and b) shocked quartz garins are found at brecciated glassy texture easily changed with feldspar grains with twinning from original texture.

Water analysis: Water analysis from the crater bottom of 1,750m indicates that temperature is 45 degree C, and rich in Na+, Cl□ and Fe(total) ions, and F ions, though there is no S ions (as in the volcanic hot spa in Japan) which was analysed by official hot-spa Laboratory of Kagawa Prefecture Laboratory. This indicates that water from buried crater bottom is not volcanic type, but non-vocanic,deep-layer grandwater and fossil sea-water type water which can be applied for hot-spa.

Broken buried crater structure: There is "no active and large volcanic rocks" at drilled samples under 450m of real crater sediment and crater bottom which suggest that there is "no large volcanic event" in the crater formation. Later volcanic intrusions along cracks are considered to be a) young volcanic rocks from small intrusion of andesite after crater formation, and b) rocks injected to the cracks of buried crater structure which were formed by later Goshiki-dai basaltic

intrusion. The latter broken process is considered to be formed at a) uplifts of Granitic basements, and b) basaltic intrusion of the Goshikidai plateau produces finally compression to South-East direction to against original crater structure to form crashed granitic rocks around the crater structure (Fig.4). This process can be found by negative gravity anomaly [9] of the crater to show ellipsoidal-shape on NE-SW direction against hard granitic blocks at the South direction. Sharp negative gravity anomaly with two types of ellipsoidal shape were formed by by later crustal event of small volcanic intrusions along the crack to form quasi-circular shape of 4km in size finally. These strong broken process are found from field outcrop observation that almost all Ryoke garnites found in and around the buried crater are broken to small blocks of granitic rocks.

Summary: Drilled samples to 1,750m in depth of buried crater of Takamatsu-Kagawa district of Japan show shocked quartz and Fe-Ni-Co grains mainly crater sediments. Water from the bottom indicates non-volcanic tyoe water. Compared with other drilled samples of the volcanic Goshikidai plateau, buried crater of Takamatsu-Kagawa district is not srong volcanic type but meteoritic impact type. Large basaltic intrusions of the Goshikidai plateau squeeze original shape of the meteoritic crater structure. Small andesitic intrusions after impact event form finally smaller quasi-circular crater of half size (4km in size) [2-7].

References: [1] Miura Y. et al. (2001): *LPS XXXII* , Abstract#1981. [2] Miura Y. (2001): *Meteoritics Planet. Sci.* 36S, 136-137. [3] Miura Y. et al. (2001): *Proc. 34th ISAS LPS* ,33,183-186. [4] Miura Y. (2002): *Geol. Soc. America (Denver,USA)*, Abstract 239-11, [5] Miura Y. (2002): *LPS XXXIII*, Abstract# 1231. [6] Miura Y. (2002): *Meteoritics Planet. Sci.* 37S, 101. [7] Miura Y.(2002): *Proc. 35th ISAS LPS* ,34,124-127. [8] Miura Y.(2002): NIPR 25th Antarctic Meteorites. [9] Furumoto M.,Y.Miura & Y.Kono (1996): *Proc. Int. Symp. Obs. Cont. Crust through Drilling*, 8, 172-177.

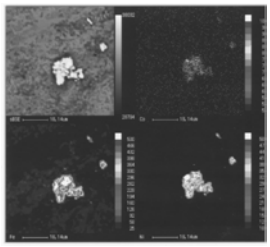

Fig.2. Electron color-mapping micrographs of Fe-Ni-Co-bearing particles with SEM image (upper left) at 610m drilled sample of buried crater in Takamatsu-Kagawa district in Japan [4-8]

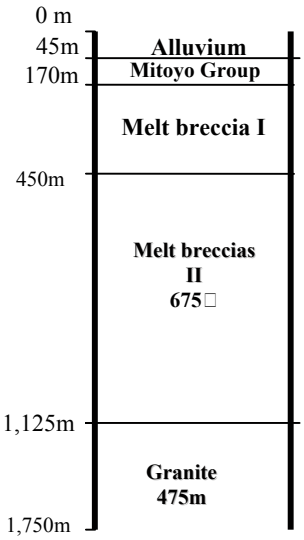

Fig.1. Drilled log of buried crater structure at the Takamatsu-Kagawa district in Japan [4-7].

.

Fig.3. Optical polarized micrograph of shocked quartz
Multiple sets of the PDFs texture with three directions in breccias at buried crater in Takamatsu-Kagawa district , Japan [4-8].

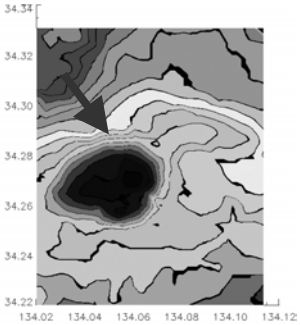

Fig.4. Gravity anomaly mapping of Takamatsu-Kagawa district (Center as dark area), together with volcanic Goshikidai compressuion from NW direction shown by arrowm [4-8].

POSSIBLE IMPACT CRATERS IN CHINA: PRELIMINARY REPORT, Y.Miura, T.Maeda[1], J.B.Li [2,3], A.Nakamura[1],and X.Hu[2]. 1Dept. of Earth Sci., Faculty of Sci., Yamaguchi University, Yoshida 1677-1, Yamaguchi , 753-8512, Japan. yasmiura@yamaguchi-u.ac.jp. 2.President Office, University of Qinghai, Xining, Qinghai, 610016, P.R.China. 3.The State Key Lab. NCFR, Tsinghua University, Tsinghua, Beijing, 100084, P.R.China.

Introduction: There are few reports of impact crater in China, because large China continents consists of a few smaller continents by continental drift including Japanese old basements from southern parts of the Equator [1,2]. Japanese first impact crater research [3-6] can be applied to survey first China impact crater. In fact, senior author used Yamaguchi University academic fund of China - Japan Academic Exchange of 2002FY, to collect the samples at candidates of Chinese crater one month of summer holiday period o 2002. From satellite images and geological maps, we visited eight locations of wide China country to find best candidates of China crater region of Qinghai Province, western highlands of China. Purpose of the present paper is to discuss

Possible impact craters in China from geological - topographic maps and satellite images.

First candidate of Chinese craters in Qinghai Province: We found best candidate of Chinese impact craters in highlands of 2,200m to 4,000m in height, where old peoples (>60 years old) are not welcome mainly due to its less oxygen region. There are few active volcanic rocks, but primordial basement rocks of granitic and gneiss rocks are found. The following three possible craters are selected here from satellite images, rock collections and material analyses :

1) Possible impact crater A: Black and red impact-like melt breccias are collected at south and north sides, respectively, of the Qinghai Lake, Qinghai Province, P.R.China. Brecciated rocks are found at western part of the lake. Shattercone like texture on black shale can be found at west and east sides of the lake. Present large lake (ca.60kmx30km) shows irregular shape where fault line to form low lands are crossed to the center of the lake during Chinese joining from a few smaller continents. The Qinghai Lake is the largest salt-rich lake in China, which reveals strange water circular system to flow out to the bottom of the lake (maybe along the crack lines). Therefore, its lake is considered to be joint lakes from three small lakes (ca.10km in size) by tectonic movement of the joining to form larger lake.
2) Probable impact crater B: satellite image photo shows quasi-circular structure with central peaks as ca.20km in size in Qinghai province, P.R. China. The north and south rims of the crater structure reveal black and red impact melt rocks, respectively. This crater structure is broken by radiated direction with three rivers and fault lines which were formed by crustal movement after impact event.
3) Clear impact crater C: Photographic image shows clear rim and with central peak of the lake in Qinghai Province, China. The detailed sampling will be planned next summer holiday period.

Impact melt rocks: There are two impact melt glasses (i.e. tektites) by impact process are found first in Qinghai Province,

1) Impact glass rock I: It reveals glassy silicate rocks found at north of the possible impact crater B in Xining city of Qinghai Province.
2) Impact glass brecciated rock II: This is mixed with brown clasts and red matrix glasses which is considered to be formed at possible impact crater A.

Summary: There are three candidates of Chinese impact craters with impact melt rocks (found two crater candidates). The more detailed survey and analyses will be planned as joint cooperation project.

References:[1] Y.Miura and S.Tanaka (2003):*In this LPI Contribution*. pp.1 (submitted). [2] Y. Miura, M.Kedves and J.Rucklidge(2001): *Proc. 23th ISAS Solar System* ,23, 13-16. [3] Miura Y. (2002): *Geol.Soc.America (Denver,USA)*, Abstract #239-11, [4] Miura Y. (2002): *LPS XXXIII*, Abstract# 1231.[5] Miura Y. .(2002): *Proc. 35th ISAS LPS* ,34,124-127. [6] Y.Miura (2003):*In this LPI Contribution*. pp.1 (submitted)

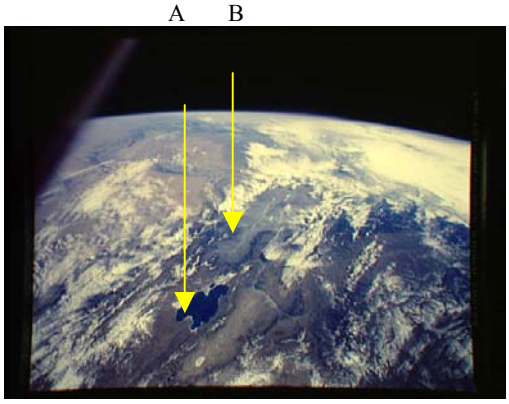

Fig. 1. Satellite image (NASA, Space Shuttle) of possible impact craters in Qinghai Province, P.R.China. Thanks for NASA satellite images.

LATE DEVONIAN ALAMO EVENT, NEVADA, USA; MULTIPLE EVIDENCE OF AN OFF-PLATFORM MARINE IMPACT. J. R. Morrow[1] and C. A. Sandberg[2], [1]Department of Earth Sciences, University of Northern Colorado, Greeley, CO 80639, USA, jared.morrow@unco.edu, [2]Geologist Emeritus, U.S. Geological Survey, Box 25046, MS 939, Federal Center, Denver, CO 80225, USA, sandberg@usgs.gov.

Introduction: The early Late Devonian (early Frasnian) Alamo Event is proven to have resulted from a marine impact [1–3] into interbedded carbonate and siliciclastic target strata offshore from the carbonate-platform margin [4, 5]. Post-Event geologic processes along the tectonically active western North American continental margin, however, have dismembered and buried the 1.5-km-deep, 50- to 75-km-wide crater. Allochthonous and semi-autochthonous polymict breccias, impact ejecta, and seismically disturbed strata resulting from the impact are now exposed in more than 20 mountain ranges in southern and central Nevada and western Utah, USA (Fig. 1). Megabreccia and tsunamite deposits were emplaced in: (a) roughly semicircular, shoreward-thinning belts, designated Zones 1, 2, and 3, across the carbonate platform and adjacent ramp; (b) localized, erosive, crater-fill channel or sheet deposits that downcut into deep-water ramp and slope strata as old as Middle Devonian (e.g., MLK, RMW, SKR, and CW, Fig. 1); and (c) distal, fine-grained, possible uprush-related channels on the inner carbonate platform (e.g., DVG, Fig. 1).

Impact-Related Phenomena: Since recognition of the impact origin for the Alamo Breccia and related Event deposits [1-3], there has been a growing body of evidence documenting the magnitude, paleogeographic setting, chronology, and distal effects of the impact. At present, in the absence of a preserved crater, at least 15 separate lines of geologic, petrographic, and geochemical evidence demonstrate that the Alamo Event was caused by a relatively large cometary impact into a deep-water, off-platform marine setting. Existing evidence further demonstrates that the ensuing target vaporization, platform collapse, transient-crater modification, megatsunami, and ejecta emplacement followed a complex, multi-stage evolution. Important lines of evidence documenting an impact genesis for the Alamo Event include:

(1) Megabreccia – Size, location, and distribution of radially imbricated blocks and megablocks in Zone 2 and in offshore, deep-water channel deposits of the Alamo Breccia [1, 3, 4, 6].

(2) Clastic dikes and sills – Extending at least 300 m stratigraphically beneath the Breccia; provided conduits for mobilization and upward injection of quartz sand grains from underlying partly consolidated siliciclastic strata [1-4].

(3) Lateral shock waves – Detachment surfaces beneath semi-autochthonous, platform megabreccia blocks in Zone 2 [1-3], disruption and plastic deformation of sub-Breccia units in Zone 1 [1, 3], and probable seismites in the distal platform setting where the Breccia is absent [4].

(4) Megatsunami deposits – Multiple, stacked event beds capping the Breccia in Zone 2 and in offshore channels [1-3], stranded uprush deposits in Zone 3 [1-3], and possible distal uprush channels [2, 4].

(5) Iridium anomaly – High relative abundance above background levels, but low absolute concentration (average value ~70 ppt) [3, 7], suggesting a probable cometary impactor.

(6) Shocked quartz grains – Abundant within onshore and offshore deposits of the Breccia, sub-Breccia clastic dikes and sills, and carbonate accretionary lapilli; showing Planar Deformation Feature (PDF) distribution and orientation diagnostic of sedimentary target shock metamorphism [1, 3, 5, 7-9].

(7) Ejected, redeposited conodont microfossils – Within the upper part of the Breccia, occurring in association with carbonate accretionary lapilli and other ejecta fragments; indicating that crater excavation penetrated deep into Lower Ordovician strata 1.5 km beneath the early Late Devonian seafloor [1, 2, 4, 5].

(8) Carbonate accretionary lapilli – Impact-fallout spherules, produced by condensation of vaporized carbonate rock, which occur in the upper part of the Breccia as isolated grains and in normally graded blocks that had been partly cemented shortly after deposition; subsequent megatsunami fragmented, reworked, and redeposited the lapilli beds as blocks [3, 7].

(9) Ejecta bomb – Spindle-shaped, zoned impact-fallout projectile within an offshore Breccia channel at Milk Spring (MLK, Fig. 1), showing evidence of a complex accretional history during ballistic aerial transport [10].

(10) Distal ejecta – Isolated occurrences of inclusion-rich quartz grains containing abundant planar fractures and rare PDFs at a stratigraphic level correlative with the Alamo Event, but where the Alamo Breccia may not have been deposited or preserved (e.g., NAR and CON, Fig. 1) [5, 9, 10].

(11) Glassy melt grains – Isolated within the Breccia matrix and occurring within the ejecta bomb are cryptocrystalline, partially isotropic spherical and aggregate grains, which may represent original silicate melt ejecta [10].

(12) High-pressure quartz polymorphs – Small, optically high-relief crystals are a common feature within highly decorated, mono- and poly-crystalline Alamo shocked quartz grains; although not yet confirmed by other quantitative methods, these crystals may be the high-pressure quartz polymorph coesite.

Conclusions: Given the high probability that craters from pre-Pangea oceanic impacts may not be preserved in the geologic record, other converging lines of evidence, such as those documented for the Alamo Event, must be used to recognize and correctly catalogue ancient marine impacts.

Evidence compiled for the Alamo Impact documents the great magnitude and wide extent of the Event within onshore, offshore, and distal settings. Resulting breccias are now recognized at least 100 km from the inferred impact site, and distal quartz ejecta, as distant as 250 km. We interpret offshore deposits of the Alamo Breccia to be large, submarine mass-flow channels or sheets that were emplaced both by high-energy, outward- and downslope-directed surge currents/tsunami originating at the Alamo Impact site and by inward-directed return currents backfilling the unstable transient crater. The complex internal stratigraphy of both onshore and offshore Breccia indicates that post-impact platform collapse, submarine mass-flow, and resulting megatsunami may have played an important role in modifying the initial Event deposits. On the basis of the multiple lines of evidence now recorded, we conclude that the Alamo Event resulted from a relatively large (~5-km-diameter) cometary impact into a deep-water, oceanic target west of the early Late Devonian carbonate platform.

Acknowledgments: J.E. Warme, A.C. Chamberlain, H.-C. Kuehner, F.G. Poole, and W. Ziegler are gratefully acknowledged for their contributions to our expanding knowledge and understanding of the Alamo Event.

References: [1] Warme J.E. and Sandberg C.A. (1995) *CFS 188*, 31-57. [2] Sandberg C.A. et al. (1997) *BYU Geol. Stud*., *42:1*, 129-160. [3] Warme J.E. and Kuehner H.-C. (1998) *IGR*, *40*, 189-216. [4] Morrow J.R. et al. (2001) *LPI Contr. 1080*. [5] Sandberg C.A. et al. (2002) *GSA Spec. Pap. 356*, 473-478. [6] Morrow J.R. et al. (2002) *GSA Abs. Prog*., *34:4*, A-52. [7] Warme J.E. et al. (2002) *GSA Spec. Pap. 356*, 489-504. [8] Leroux H. et al. (1995) *Geol., 23:11*, 1003-1006. [9] Morrow J.R. and Sandberg C.A. (2001) *LPI Contr. 1080*. [10] Morrow J.R. and Sandberg C.A. (2002) *GSA Abs. Prog*., *34:6*, 543-544.

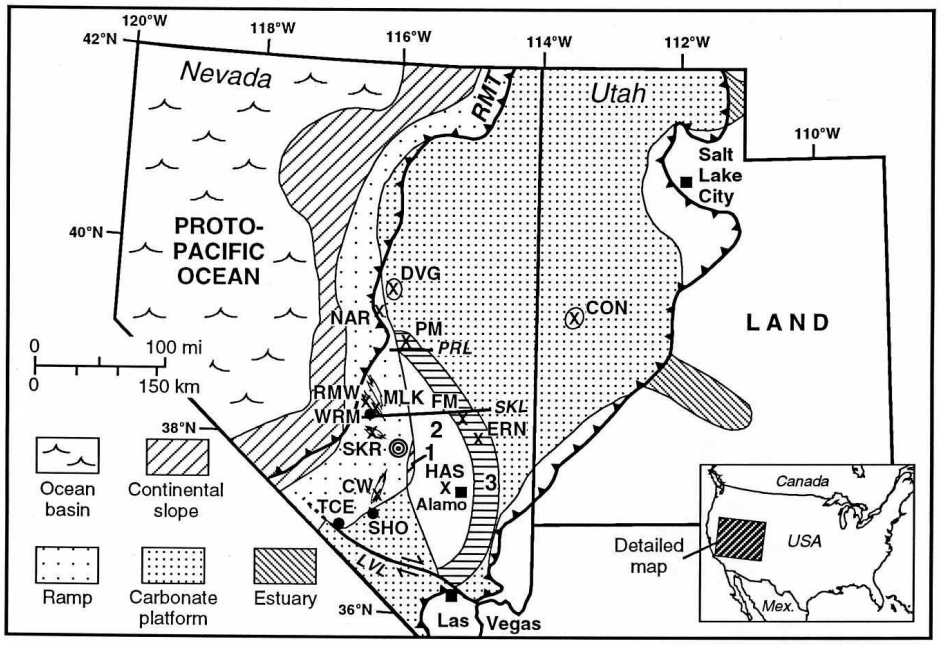

Figure 1 – Paleotectonic map (partly restored) of Nevada and Utah during early Frasnian *punctata* Zone, showing possible site of oceanic Alamo Impact (bullseye) relative to carbonate platform and distribution of resulting Alamo Breccia and related deposits. Alamo Breccia Zones 1, 2, and 3 form semicircular pattern on ramp (Zone 1), outer carbonate platform (Zone 2), and peritidal, inner platform (Zone 3). Also shows location of four deep-water channels of Alamo Breccia, some representing crater fill and some transporting breccia debris seaward. Selected major post-breccia structural features: ***RMT***, latest Devonian to Early Carboniferous Roberts Mountains thrust, which significantly displaced transitional- and oceanic-facies Devonian rocks; and three Tertiary lineaments that affected distribution of Alamo Breccia – ***LVL***, Las Vegas lineament; ***SKL***, Silver King lineament; and ***PRL***, Pancake Range lineament. Important measured sections: **CON**, Little Mile-and-a-Half Canyon; **CW**, Carbonate Wash; **DVG**, Devils Gate; **ERN**, East Ridge North; **FM**, Fox Mountain; **HAS**, Hancock Summit (type locality of Alamo Breccia); **MLK**, Milk Spring; **NAR**, Northern Antelope Range; **PM**, Portuguese Mountain; **RMW**, Rawhide Mountain West; **SHO**, Shoshone Mountain; **SKR**, Streuben Knob; **TCE**, Tarantula Canyon East; **WRM**, Warm Springs. Alamo Breccia localities are indicated by X's; other important localities are indicated by dots. DVG and CON deposits are unclassified. Modified from [5].

MASS TRANSFER IN LARGE BOLIDE IMPACTS: GEOCHEMICAL EVIDENCE FROM THE SUDBURY STRUCTURE. J. E. Mungall[1], J. J. Hanley[1], D. E. Ames[2]. [1]Dept of Geology, University of Toronto, 22 Russell St, Toronto ON M5S 3B1, Canada. [2]Mineral Resources Division, Geological Survey of Canada, 601 Booth St, Ottawa, ON, K1A 0E8.

The redistribution of matter in the lithosphere resulting from large bolide impacts affected the development of the early crust and upper mantle of the Earth and other terrestrial planets. Here we present rock composition data from the Sudbury impact structure representing magmatic liquids quenched shortly after the time of impact in environments spanning a stratigraphic column several kilometers high. Shock-melted lower crustal material has been elevated to the surface of the Earth to form a melt-sheet now preserved as the Sudbury Igneous Complex, effecting a regional overturn of the gross compositional stratification of the continental crust. Impact melt breccia from the lower crust has been injected along dikes and faults for distances of tens of kilometers throughout the brecciated upper crust. Fallback deposits of the Onaping Formation have compositions similar to that of the underlying melt-sheet but are zoned upward to reflect increasing contributions both from the original surficial sedimentary strata and from the impactor.

Our work has implications for the crustal-scale redistribution of matter during large impact events, which controlled the stability and longevity of the crust during the Hadean Eon. The retention of impactor and supracrustal material in the uppermost portion of the impact-related stratigraphy is consistent with their having been ejected upward by the explosion of the impactor and target rocks after the impactor had implanted itself several km into the target crust. It thus appears that the impacting body did not remain within the crust, but was redeposited as a veneer at the Earth's surface mixed into the uppermost target rocks. Below this veneer, molten rock from the lower crust or mantle was elevated to the level of the upper crust, overlying the former rocks of the upper crust and effecting a major compositional overturn in the lithosphere. Offset dikes and Sudbury breccias record a process of injection of melted or otherwise disaggregated lower crustal material for distances of several tens of km laterally and upward from the zone of deep crustal melting into their present positions structurally beneath and adjacent to the Sudbury Igneous Complex. Intense meteorite bombardment might have repeatedly overturned the lithsphere, hindering the stabilization of continental crust until the normal run of impact melting events was too shallow to reach significantly below the base of the crust.

Probing the Sudbury Structure at Depth - An ICDP Proposal. J. Mungall[1], B. Milkereit[2], R. Grieve[3] and C.M. Lesher[4], [1]University of Toronto, Canada, [2]University of Toronto, Dept. of Physics, 60 St. George St., Toronto, Canada, M5S 1A7, bm@physics.utoronto.ca, [3]Natural Resources Canada, Ottawa, Ontario, [4]Mineral Exploration Research Centre, Laurentian University, Sudbury, Ontario.

Introduction: The Sudbury structure is the largest and best-exposed remnant of a large meteorite impact struture on earth. It hosts one of of the world's largest concentrations of magmatic Ni-Cu-Pt-Pd-Au minerazations and has produced more than $100 billion worth of metal in over a century in production. It is a unique example of a large differentiated igneous body with remarkably simple boundary conditions (Fig. 1). As such it is the premier location on earth to study processes related to impactand planetary accretion, as well as a wide range of magmatic processes including the generation of large magmatic sulfide deposits. It is proposed to conduct a comprehensive program of research into the genesis and evolution of the Sudbury Structure centered on a scientific drilling program.

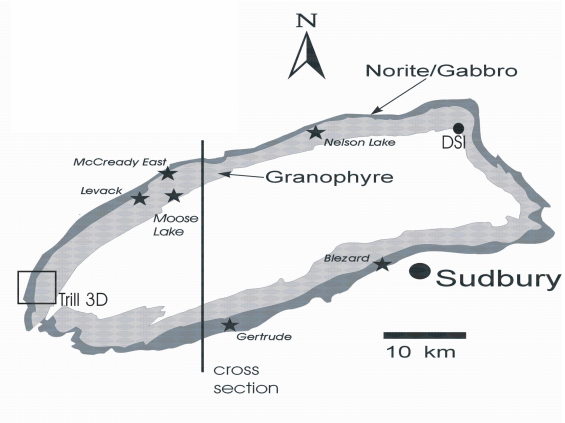

Fig. 1. Location map of the Sudbury Igneous Complex (SIC) with borehole locations and cross section shown in Fig. 2.

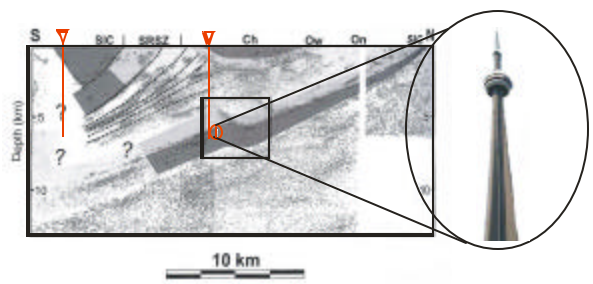

Fig. 2. North-South cross section of the Sudbury structure with potential deep drilling locations. CN Tower of 550 m for scale.

Geophysical Database: Since 1988, an extensive database of 2D and 3D seismic surveys, borehole geophysical logs, and petrophysical studies on core samples has been assembled for the Sudbury Structure [1-6,8]. Seismic reflection data show the deep geometry of the Sudbury Structure to be markedly asymmetric. In terms of seismic exploration, the contact between the "transparent" Sudbury Igneous Complex (SIC) and the "reflective" footwall complex represents a clear regional marker horizon, making it possible to map the bottom of the SIC. In addition, prominent reflections are observed from within the Whitewater group (at the Chelmsford-Onwatin and Onwatin-Onaping contacts)[5,8]. No significant difference in acoustic properties is observed along strike between North and South Range [1,6].

Asymmetry and Shortening of the Sudbury Structure: Integrated geophysical and rock property studies of the Sudbury Structure have revealed it is highly deformed with substantial NS shortening in the SIC (Fig. 2). There is a remarkable transition in the underlying cause of seismic reflectivity in less than 30 km between the North Range and the South Range [2,3]. Major, relatively continuous reflections in the North Range correlate with lithologies exposed in drill holes and at the surface. The Norite layer of the SIC and the underlying highly reflective footwall complex can be traced as a southward dipping unit from outcrop in the North Range to a depth of 10 km beneath the southern rim of the SIC. In contrast, the South Range seismic data are dominated by reflections from shear zones and other tectonized structures in the South Range Shear Shear Zone (SRSZ), a broad zone of pervasive ductile shear [7]. The broad zone of intensive ductile deformation transects the Paleo-Proterozoic SIC and likely formed during the final stages of the Penokean orogeny on the southern margin of the Superior Province. Seismic data reaveal a three-dimensional image of this deformation zone. The seismic image of the deformation is best developed within the Onaping formation; the southern edge of the seismically imaged shear zone does not extend significantly beyond the exposed SIC, suggesting lateral limits to the deformation in the Sudbury Structure. From the location of drillhole intersections it

is clear that the thrust faults record a displacement magnitude of at least 1.8 km from the SSE [3].

Seismic reflection data from the North Range show that the Norite and underlying highly reflective footwall can be traced southward from outcrop to a depth of at least 5 km beneath the center of the Sudbury Basin. Beneath the center, a dramatic change in the dip of the contact and the thickness of the Norite is observed [2,5,8]. The thick Norite is located structurally below the most intense deformation associated with the SRSZ.

The change in dip and depth of the Norite layer beneath the center of the Sudbury Basin at 5 to 6 km depth require further study. It is worth noting that a controlled source electromagnetic has revealed a prominent conductive zone within/beneath the SRSZ and above the thick Norite. In addition, local gravity and magnetic anomalies are bcated above the thick Norite[2,4]. Lithological determinations beneath the SRSZ remain problematic and the physical mechanism for the geophysical anomalies need to be studied.

Scientific Drilling Proposal: A deep drilling project (one to three boreholes, slim-hole drilling to depth of about 6 km, continuous core recovery) was submitted to the International Continental Drilling Program (ICDP); it will offer information regarding the overall architecture of the Sudbury Structure [9]. Initial down-hole geophysical probes will be replaced by a long-term semi-permanentdown-hole laboratory including equipment for seismic surveys, fluid and gas sampling, monitoring the state of stress. Basic geophysical measurements will provide quantitative constraints on conditions likely to be encountered during the inevitable push to extract ore from depths as great as 4 km. The drilling project needs to be fully integrated into a regional synthesis of geological data.

References: [1] Adam, E., Perron, G., Milkereit, B., Wu, J., Calvert, A.J., Salisbury, M., Verpaelst, P. and Dion, D.J., (2000) Can.J.Earth. Sci, 37, 503-516. [2] Boerner, D.E., Milkereit, B., and Naldrett, A.J., (1994) Geophys. Res. Letters, 21, 919-922. [3] Boerner, D.E., Milkereit, B., Wu, J. and Salisbury, M., (2000) Tectonics, 19, 397-405. [4] Boerner, D.E., Milkereit, B. and Davidson, A., (2000) Can.J. Earth Sci, 37, 477-501. [5] Milkereit, B., Green, A. and the Sudbury Working Group, (1992) Geology, 20, 807-811. [6] Milkereit, B., Berrer, E.K., King, A., Watts, A.H., Roberts, B., Adam, E., Eaton, D.W., Wu, J. and Salisbury, M., (2000) Geophysics, 65, 1890-1899. [7] Shanks, W.S. and Schwerdtner, W.M., (1991) Can.J.Earth.Sci, 28, 411-430. [8] Wu, J., Milkereit, B., and Boerner, D.E., (1995) J.Geophys. Res., 100, 4117-4130. [9] Mungall, J., Milkereit, B., Grieve, R. and Lesher, M., (2003) Scientific Drilling of the Sudbury Structure, ICDP Proposal.

SULFIDE MINERALIZATION IN THE 100-KM POPIGAI IMPACT STRUCTURE, RUSSIA. M.V. Naumov, V.D. Lyakhnitskaya, O.A. Yakovleva. Karpinsky All-Russia Geological Research Institute (VSEGEI), 199106 Sredny pr., St.Petersburg, Russia, mvn@mail.wplus.net

Introduction. The presence of the world class Ni-Cu-PGE sulfide ores in the Sudbury impact structure [1, 2] has driven efforts to study the distribution of sulfides in other large impact craters. In this aspect, the 100-km Popigai impact structure (Northern Siberia, Russia) is of particular interest due to the occurrence of a wealth of impact melt rocks (~3000 km^3); this amount is the largest for terrestrial craters except the Sudbury.

The Popigai crater originated 35.7 Ma ago in two-layered target, which is composed of Archean and Lower Proterozoic crystalline rocks overlain by 1.5-km sequence of Upper Proterozoic, Paleozoic, and Mezozoic sediments. The crater fill consists of impact melt rock (massive, tagamite, and fragmental, suevite) and lithic breccia up to 2 km of total thickness. Some lense-like bodies of high-temperature (HT) and low-temperature (LT) varieties can be distinguished within thick tagamite sheets [3].

In this study, we explored spatial range and composition of the sulfide mineralization across the whole area of the Popigai crater, as well as in vertical sections through thick impact rock sequences. Although the sulfides are present in all impact lithologies, scattered dissemination or thin veins alone were found. Sulfides and associated minerals were studied using optical microscopy, X-ray diffractometry, electron microprobe analysis; some atomic emission spectroscopy and sulfur isotope measurements of sulfide separates were also carried out. Besides the concentrations of both major and trace elements in the impact melt rocks and target rock samples were measured; major elements were determined by XRF and trace elements by ICP-MS.

Distribution of the sulfide mineralization. Three genetic groups of sulfide associations are distinguished: (1) pre-impact, (2) syngenetic, (3) epigenetic.

Pre-impact sulfides. Disseminated and vein mineralization occurs in all target lithologies, i.e., shocked and brecciated gneisses, amphibolites, dolerites, dolomites, aleurolites, etc. Following a diversity of the target, this group is characterized by a wide variety of sulfides. Pyrrhotite and pyrite are predominant as a whole; in addition, sphalerite, galenite, molybdenite, millerite, zigenite, arsenopyrite, marcasite, melnikovite, and altaite are identified in places. Sulfides are of considerable importance in target rocks in some zones of brecciation on the crater rim in the southwestern sector alone, where relics of a metalliferous millerite-pentlandite-chalcopyrite association are established along the boundaries of lense-like ultrabasite bodies. Pre-impact sulfides are modified to a variable extent by impact-enhanced cataclasis, thermal methamorphizm and hydrothermal alteration. As a result, an original pyrrothite is replaced by pyrite-marcasite aggregate. Secondary sulfides are more abundant in Ni than original ones (Ni contents up to 1,5% and 0,34%, correspondingly).

Syngenetic sulfides were formed by impact melt crystallization. They are represented mainly by pyrrhotite droplets (up to 4 cm in size, but commonly <0,1 mm) and euhedral grains dispersed in tagamites and impact glasses. Minor pentlandite and chalcopyrite are included locally in pyrrhotite. In some places, a secondary pyrite-sphalerite-galenite association occurs in tagamites. HT- and LT-tagamites differ in both structural modification of the predominant ferroan monosulphide (hexagonal pyrrhotite and troilite in HT and monoclinic pyrrhotite in LT) and Co/Ni and (Ni+Co)/Fe ratios in pyrrhotite, the fact fixing the distinction of conditions of sulfide crystallization in impact melts. Ni and Co contents in pyrrhotite vary strongly (from 0 to 2,79% and from 0 to 0,40% correspondingly), as well as the Co/Ni ratio. Accessory sulfides (chalcopyrite, pentlandite, sphalerite) in tagamites are distinct in their composition from pre-impact sulfides.

Epigenetic sulfides are derived from the impact-generated hydrothermal circulation. They are represented by pyrite with minor chalcopyrite and sphalerite. Pyrite together with calcite and zeolites form filling veins in impact rocks and aggregate epimorphoses after clasts of coaly shales, argillites, siderites, etc. in suevites and lithic breccias. The latest pyrite generation develops in subvertical fractures in tagamites. Epigenetic pyrite occurrences are characterized by the strong preference of cuboctahedral habit of crystals and by enrichment in Ag, As, Zn and depletion in Ni, Cu, Co as compared with syngenetic sulfides.

Geochemistry of impact melt rocks. Both major and trace element data (including REE) suggest the compositional homogeneity of the impact melt throughout the Popigai structure. Trace element concentrations in tagamites show small variations (no more than 3-4 times) in abundances. From ICP-MS data, an average tagamite contains 48 ppm Ni, 15 ppm Co, 30 ppm Cu, 14 ppm Pb, 68 ppm Zn, 0,73 ppm Ag, 0,01 ppm Au, 0,02 ppm Pt, 0,47 ppm Pd. Compared to the target rocks, the tagamites are slightly enriched in Ni, Cu, Mo, V, Cr, Mn, Zn. Nickel, cobalt, and molybdenum contents show the spatial distribution but in vertical sections through thick tagamite sheets no regular variations in metallogenic element contents are detected. Both tagamites and suevites have low sulfur contents (0,02-0,07 wt.%), which are lower as mush as 1,5-2 times than in target crystalline rocks. Unlike target rocks, a positive correlation between sulfur and siderophile elements (Fe, Ni, Co) abundances is revealed for tagamites; consequently, the sulfur fixes predominantly as sulfide in the course of the impact melt crystallization.

Sulfur isotopes. The sulfur isotope composition of ten sulfide samples from impact melt rocks and of six sulfide samples from target rocks has been measured at the Vernadsky Institute of Geochemistry, Moscow. Both syngenetic and epigenetic sulfides have a narrow $\delta^{34}S$ range of –2,4‰ to 3,4‰ CDT, while the sulfides from crystalline target rocks have values of +1,3‰ to 3,7‰ CDT.

Conclusions. 1. The Popigai impact event produces two genetic types of sulfide associations: (1) a syngenetic low-sulfur mineralization in the impact melt and (2) an epigenetic high-sulfur mineralization in diverse impact lithologies. Taking into account some data on sulfide mineralizations from other craters (Kara, Puchezh-Katunki, Suavjärvi, etc), analogous types can be distinguished as characteristic of terrestrial impact structures at all including Sudbury, these are: (1) a syngenetic Co-Ni-Cu mineralization (pentlandite-chalcopyrite-pyrrhotite) and (2) a hydrothermal Cu-Pb-Zn-Ag mineralization (galenite-sphalerite-chalcopyrite-pyrite).

2. Based on the common spherical shape of sulfide segregations in impact melt rocks, the liquid immiscibility is proposed for the formation of syngenetic sulfides. Since the impact melt was unsaturated in sulfur, a low-sulfur monosulfide solid solution was crystallized. In LT-tagamites, the bulk of original sulfide segregations was recrystallized during the secondary alteration.

3. Inferred from the sulfur isotope data, the sulfides from impact melt rocks arise at the expense of pre-impact sulfides. This is confirmed by evidences from some other terrestrial craters, especially from Kara where the $\delta^{34}S$ values in sulfides from impact melt rocks (-10‰- to -12‰ CDT) are similar that of pre-impact sulfides, which are strongly depleted in heavy sulfur .

4. Although there is a vague similarity between Popigai and Sudbury in average impact melt compositions and in principal features of the appearance of sulfide associations, no sulfide concentrations are found in the Popigai. This difference may be attributed to (1) a lesser amount of the impact melt, (2) a lack of evidences for melt differentiation (both original and crystallization), (3) an absence of metallogenic specialization of the target, (4) a low intensity of the post-impact hydrothermal processes, (5) a burial of base horizons of impact melt sheets beneath thick impact ejecta blankets.

Acknowledgement. This work was supported by the Committee of Natural Resourses of the Taimyr District, Russia.

References. [1] Pye E.G., Naldrett A.J. and Giblin P.E., eds (1984). The Geology and Ore Deposits of the Sudbury Structure. Ontario *Geol. Surv. Spec. Vol., 1*, 604 p. [2] Lightfoot P.C., Naldrett A.J., eds (1994). Proceedings of the Sudbury-Norils'k symposium. *Ontario Geol. Surv. Spec. Vol., 5*, 423 p. [3] Masaitis, V.L. (1994). *Geol. Soc. Am. Spec. Pap., 293*, 153-162.

COMPARISON STUDY OF LAYERED EJECTA MORPHOLOGIES SURROUNDING IMPACT CRATERS ON GANYMEDE AND MARS. J. Neal and N. G. Barlow, Dept. Physics and Astronomy, Box 6010, Northern Arizona University, Flagstaff, AZ 86011-6010; ferfys@direcway.com; Nadine.Barlow@nau.edu.

Introduction: Voyager and Galileo imagery reveal that layered ejecta morphologies occur around some impact craters on Ganymede [1, 2]. Similar morphologies surrounding martian impact craters are commonly attributed to the role of subsurface ice [3, 4, 5]. We are studying the similarities and differences between the layered ejecta morphologies on Ganymede and Mars to investigate how impact into increasing amounts of target ice affect these ejecta morphologies.

Methodology: Our first step is to compare the morphometric properties of layered ejecta morphologies on Ganymede with their counterparts on Mars. We also are determining if there are regional variations in the distribution of the Ganymede features. We have identified seventy-one craters on Ganymede with layered ejecta morphologies, based on analysis of Voyager and Galileo imagery. These craters range in size from less than 10 km to over 40 km in diameter. We have classified each crater into a single layer (SL) or double layer (DL) ejecta morphology and used the published USGS geologic maps to identify the terrain unit on which each crater is superposed. We utilized the NIH Image software to measure crater diameter (D), maximum ejecta extent (EE), ejecta perimeter (P), and ejecta area (A) for each of these craters. We have calculated the lobateness (Γ), which is a measure of the ejecta sinuosity, using [6]:

$$\Gamma = P/(4\pi A)^{1/2}$$

and ejecta mobility (EM), a measure of the fluidity of the ejecta at the time of emplacement, using [7]:

$$EM = EE/(D/2)$$

Lobateness and EM were computed for each complete ejecta layer of the 68 SL and 3 DL craters. Γ = 1 indicates a circular ejecta blanket and Γ > 1 indicates a more sinuous ejecta blanket.

Preliminary Results: Evaluation of lobateness values indicates that the outer layers of the DL craters have lower media Γ than their corresponding inner layers. This is opposite of the trend seen for martian DL craters.

We also investigated Γ-latitude, Γ-diameter, and Γ-terrain relationships. Median Γ values are constrained between 1.1 and 1.2 regardless of diameter (Figure 1)—this range of values is consistent with the Γ values for SL craters on Mars. There is a very slight indication that Γ may be larger in the southern hemisphere of Ganymede than in the north, but the statistics are very poor (Figure 2).

Comparison of Γ between terrains shows that craters in undivided materials have higher median Γ values and craters in furrowed materials have lower median Γ (Figure 3). However, the Voyager images returned a higher median lobateness value than the Γ's found using the Galileo images (Table 1). When we consider only the Galileo data, we see very little variation of Γ with terrain. We are investigating possible reasons for the discrepancy between Voyager and Galileo results.

We are just beginning our analysis of ejecta mobility values. The average EM value for SL craters is 1.13, which is slightly lower than the average EM value for SL craters on Mars (1.47). The average EM for the inner layer of DL craters on Ganymede is 0.90 while that for the outer layer is 1.25. Again, these tend to be lower than the corresponding values for DL craters on Mars, which are 1.28 for the inner layer and 2.58 for the outer layer [8]. EM shows little variation with latitude (Figure 4). The highest ejecta mobility is seen for craters on grooved and scabrous terrains, suggesting the ejecta was more mobile in these regions (Figure 5).

References: [1] Shoemaker E. et al. (1982), in *The Satellites of Jupiter*, Univ. AZ Press, 435-520. [2] Belton M. J. S. et al. (1996) *Science, 274*, 377-385. [3] Carr M. H. et al. (1977) *JGR, 82*, 4055-4065. [4] Barlow N. G. and T. L. Bradley (1990) Icarus, 87, 156-179. [5] Stewart S. T. (2001) *LPS XXXII*, Abstract # 2092. [6] Barlow N. G. (1994) *JGR, 99*, 10927-10935. [7] Costard F. M. (1989) *Earth, Moon, Planets, 45*, 265-290. [8] Barlow N. G. and A. Pollak (2002) *LPS XXXIII*, Abstract #1322.

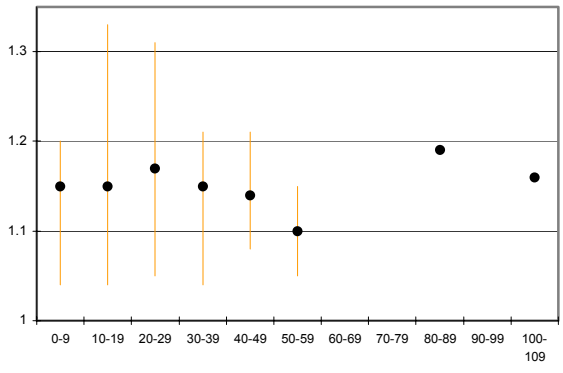

Figure 1. Γ- diameter (km) relationships. Orange

lines shows high and low lobateness values, with the black dot representing the median value.

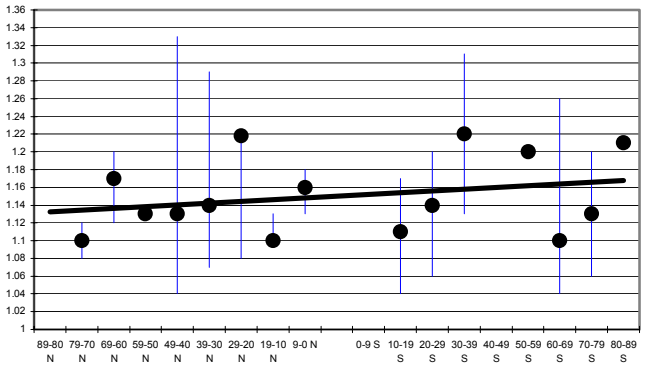

Figure 2. Γ- latitude relationships. Blue lines shows high and low lobateness values, with the black dot representing the median lobateness. A trendline is inserted to show the slight increase to the south.

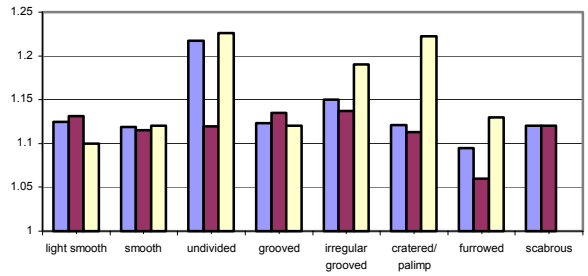

Figure 3. Γ- terrain relationships. Blue represents both Galileo and Voyager images, red represents the Galileo images and yellow represents the Voyager images.

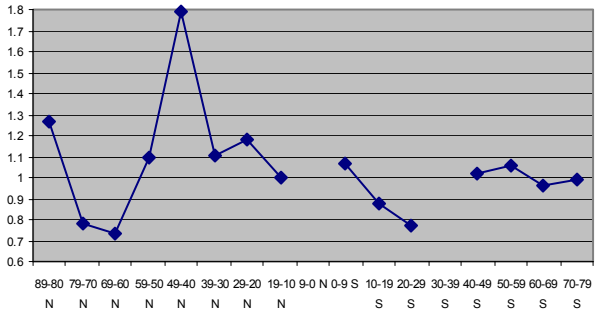

Figure 4. EM- Latitude relationships.

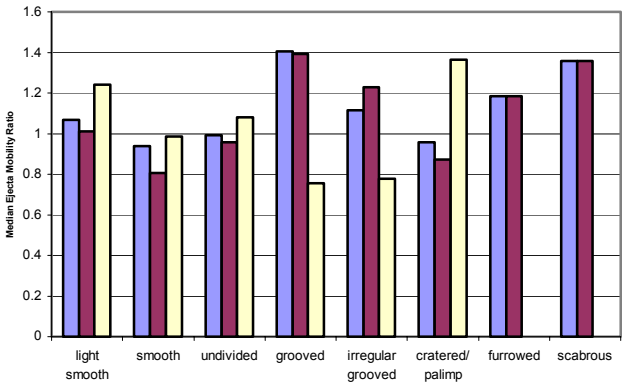

Figure 5. EM- terrain relationships. Blue represents both Galileo and Voyager images, red represents the Galileo images and yellow represents the Voyager images.

Terrain Symbol	Description	Num-ber	Mini-mum Lobate ness	Maxi-mum Lobate ness	Median Lobate-ness
1	light smooth	10	1.08	1.29	1.125
2	smooth	8	1.04	1.26	1.11875
3	undivided	17	1.04	1.31	1.217
4	grooved	14	1.04	1.33	1.123
5	irregular grooved	4	1.13	1.19	1.15
6	cratered/ palimp	12	1.06	1.21	1.1209
7	furrowed	2	1.06	1.13	1.095
8	scabrous	2	1.07	1.17	1.12
Galileo					
1	light smooth	7	1.08	1.29	1.131
2	smooth	2	1.1	1.13	1.115
3	undivided	11	1.04	1.2	1.1192
4	grooved	13	1.04	1.33	1.135
5	irregular grooved	3	1.13	1.14	1.137
6	cratered/ palimp	6	1.06	1.17	1.113
7	furrowed	1	1.06	1.06	1.06
8	scabrous	2	1.07	1.17	1.12
Voyager					
1	light smooth	3	1.08	1.12	1.1
2	smooth	6	1.04	1.26	1.12
3	undivided	6	1.2	1.31	1.226
4	grooved	1	1.12	1.12	1.12
5	irregular grooved	1	1.19	1.19	1.19
6	cratered/ palimp	6	1.06	1.21	1.222
7	furrowed	1	1.13	1.13	1.13
8	scabrous	0	N/A	N/A	N/A

Table 1. Γ - terrain statistics.

IMPACT HYDROTHERMAL ALTERATION OF TERRESTRIAL BASALTS: EXPLAINING THE ROCK COMPONENT OF THE MARTIAN SOIL M. J. Nelson and H. E. Newsom, University of New Mexico, Institute of Meteoritics, Dept. of Earth & Planetary Sciences, Albuquerque, NM 87131 U.S.A. Email: MEL14@unm.edu, newsom@unm.edu.

Introduction: The large energy in terrestrial impacts can create hydrothermal systems and consequently produce hydrothermal alteration materials. In this study we consider the chemistry of impact and volcanic hydrothermal alteration under relatively low water/rock ratios in basaltic or a somewhat more evolved protolith. Our work on the Lonar and Mistastin craters suggests that Fe-rich clays, including Fe-rich saponite can be produced. We postulate that similar alteration materials are produced on Mars and could be a component of the martian soil or regolith, contrary to some earlier studies. The martian regolith is a globally homogenized product of various weathering processes. The soil [1] is thought to consist of a "rock" component, with lesser amounts of mobile elements (Ca, Na, and K) than a presumed protolith, and a "salt" or mobile element component enriched in sulfur and chlorine [2, 3]. In this study we consider the contributions of impacts and consequent hydrothermal processes to the rock component of the martian soil.

McSween and Keil [4] investigated major element trajectories between Mars rocks and soils in an effort to distinguish between different processes that could contribute to the soil. They showed that the Mars soil is generally depleted in CaO, Na_2O and K_2O, but not FeO relative to the compositions of basaltic martian meteorites (**Fig. 1**). They concluded that this chemical fractionation is most consistent with palagonitization, the alteration of basaltic glass. Ambient temperature weathering trajectories for terrestrial basalts [5] are similar to the martian trends, but such environments are unlikely on Mars. Hydrothermal models (**Fig. 2**) that show strong iron depletion in the altered material were considered unsuccessful, along with the acid-fog model that involves leaching of the mobile elements by acids produced from the deposition of S and Cl by volcanic aerosols [6]. However, the hydrothermal data used in the comparison by McSween and Keil was based on a study of ocean floor basalts [7], leading us to look for more appropriate analogues. Our work on material altered by impact hydrothermal processes, and the recent publication of data for the alteration of terrestrial basalts under low water/rock ratios provides a new test of the possible contributions of hydrothermal materials to the martian soil.

Impact hydrothermal systems: We have obtained new microprobe data for alteration phases in samples from the Lonar and Mistastin impact craters, (Fig. 3) for comparison with the Mars data. The 1.8 km diameter Lonar crater, India is emplaced in basalt and is a good analogue for Martian craters [9]. The 28 km diameter, Mistastin crater contains an 80 m thick impact melt sheet [10, 11]. We also have looked a alteration material from the 24 km diameter Ries crater contains hydrothermally altered impact breccias [12], but the Ries material is complicated by the presence of carbonates in the target. The compositions of Lonar bulk rock and associated alteration clays (mainly Fe-rich saponite) are plotted in **Fig. 3**, as well as data for similar phases from Mistastin and related volcanic rocks. The impact crater materials, particularly those from Lonar, represent an incipient hydrothermal alteration under low water/rock ratio conditions [9]. Although hydrothermal processes can remove Fe, incipient alteration leads to the formation of Fe-rich clays and retention of Fe in the system. Materials that have experienced removal of Ca, Na, and K, but retained Fe-rich clays are also formed in volcanic hydrothermal systems under conditions of low water/rock ratio.

Volcanic hydrothermal processes: In addition to palagonite formation, other terrestrial volcanic occurrences may be relevant to Mars. The active Pantelleria volcanic hydrothermal system in Italy, for example contains basalt flows altered under conditions measured in drill holes [13]. The fractionation between basaltic xenoliths and iron-rich saponite alteration products produces trends involving iron enrichment, and mobile element depletion, not unlike the Martian models.

Mixing Models: Using matrix inversion, we have developed several mixing models in an attempt to match the composition of the martian regolith. Two SNC end members were mathematically "mixed" with alteration materials from Lonar, Mistastin, and Pantelleria to match the current mean Pathfinder soil composition [14]. Palagonite compositions can also produce successful models, as they are generally believed to be a component in the mars soil.

Conclusions: Although high water/rock ratio hydrothermal processes such as ocean floor alteration remove iron, the impact crater and volcanic data suggest that iron is not removed during low water/rock alteration due to the retention of Fe in the alteration phases. Therefore, hydrothermal alteration material can be Fe-rich, more subject to erosion, and can plausibly be a component of the martian soil.

References: [1] Clark, B.C. (1993) *GCA, 57*, 4575. [2] Newsom, H.E. and Hagerty, J.J. (1997) *JGR 102*, 19,345. [3] Newsom, H.E. et al. (1999) *JGR, 104,*

8717. [4] McSween and Keil (2000), *GCA 64*, 2155. [5] Nesbitt and Wilson (1992) Am Jour. Sci. 292, 740. [6] Banin, A. et al. (1997) *JGR 102,* 13,341. [7] Alt and Honnorez (1984) *Contrib. Min.Pet. 87*, 149. [8] Aiuppa et al. [9] Hagerty and Newsom *Meteoritics and Planet. Sci.*, in press. [10] Grieve, R.A.F. (1975) *GSA Bull. 86*, 1617. [11] McCormick K.A. et al., (1989) *Proc. LPSC 19*, 691. [12] Newsom et al., (1986) JGR 91, B13, E239. [13] Fulignati et al., *J. Volc. Res. 75*, 251, 1997. [14] Wänke et al., *Space Sci. Rev. 96*, 317, 2001. [15] Jercinovic, M.J. et al. (1990)*Geochim. et Cosmochim. Acta 54*, 2679. [16] Studigel, H. and Hart, S.R.(1983) *Geochim. et Cosmochim. Acta 47*, 337. [17] Robert, C. and Goffé, B. (1993) *Geochim et Cosmochim. Acta 57*, 3597.

Acknowledgements: Lonar crater samples provided by the Smithsonian Mineral Sciences Dept., and Mistastin samples provided by Richard Grieve. Research supported by the NASA Planetary Geology and Geophysics program (NAG5-8804, NAG 5-10143), H. Newsom P.I.

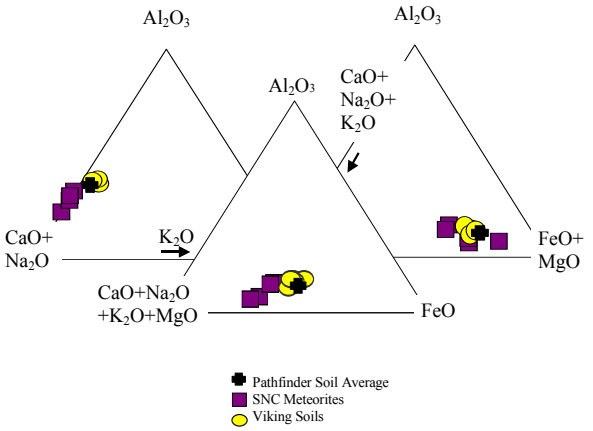

Fig.1: The mars soil appears to be somewhat depleted in CaO, Na_2O and K_2O, but somewhat enriched in FeO, relative to the rocks [4]. Weathering of basalts under ambient temperature conditions results in similar trends.

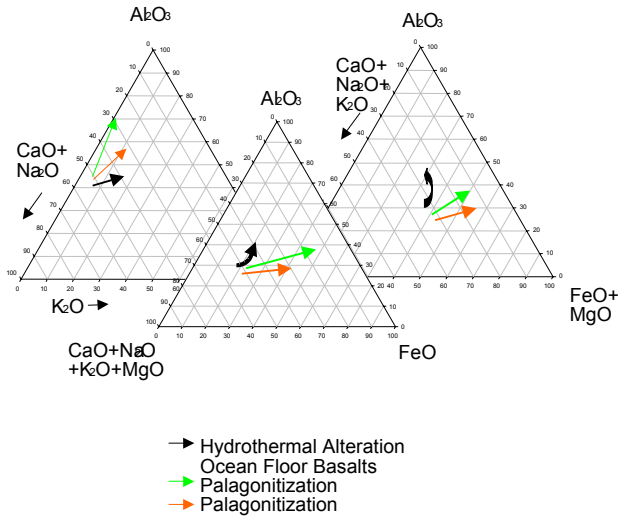

Fig. 2: Alteration trends for palagonitization [15, 16] and ocean floor hydrothermal alteration [4]. The loss of Fe during ocean floor alteration is not consistent with the martian trend.

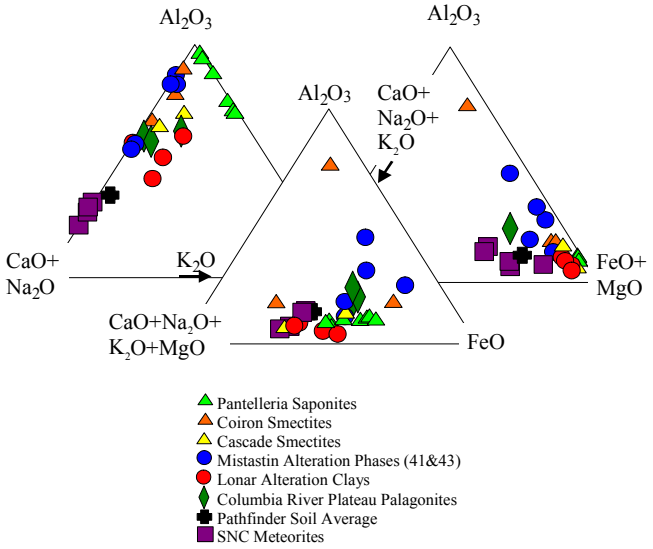

Fig. 3: Data are shown for alteration phases including Lonar crater basalt, Mistastin crater rock, and in volcanic samples from an active hydrothermal system (Pantelleria), from basalt flows into river channels (Coiron, France and Cascade, USA smectites), and palagonite from the Columbia River plateau [17].

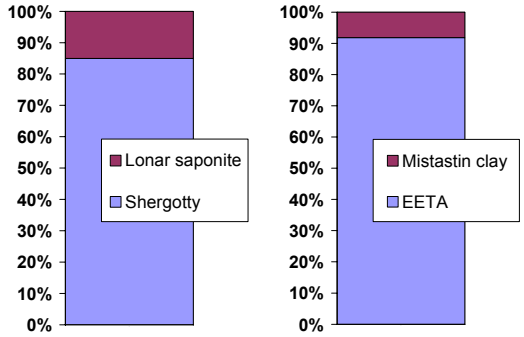

Fig. 4 Mixing model results that successfully match the composition of the "rock" portion of the martian soil with a mixture of small amounts of Fe-rich alteration material from the impact craters and basaltic martian meteorite composition materials.

EVIDENCE FOR IMPACT-INDUCED HYDROTHERMAL ALTERATION AT THE LONAR CRATER, INDIA, AND MISTASTIN LAKE, CANADA H. E. Newsom, and J. J. Hagerty, University of New Mexico, Institute of Meteoritics, Dept. of Earth & Planetary Sci., Albuquerque, NM 87131 U.S.A. Email: newsom@unm.edu

Introduction: The 50,000 year old, 1.8km diameter Lonar crater is located in Maharashtra, India [1]. This relatively small crater is of particular interest because of its unique morphological and mineralogical properties, which make it a valid analogue for similar craters on the surface of Mars [2, 3]. We show that even in this relatively small crater, substantial hydrothermal alteration of shocked breccias in the floor of the crater has occurred, probably due to the thermal effects of the impact event. The 38 my old, 28 km diameter, Mistastin crater contains an 80 m thick impact melt sheet [10, 11]. We have also documented the presence of alteration phases in the material from this larger crater.

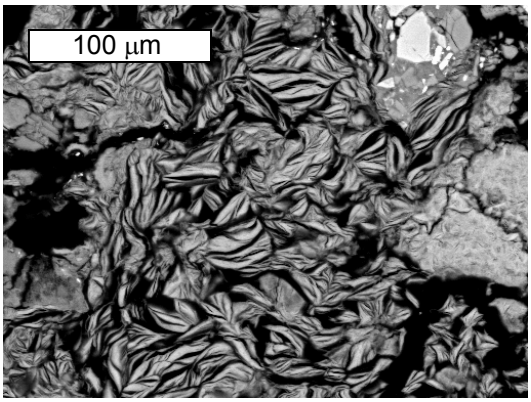

Fig. 1a. Backscattered electron image of "felty" clays in thin section NMNH 116569-13 (drill core LNR-2).

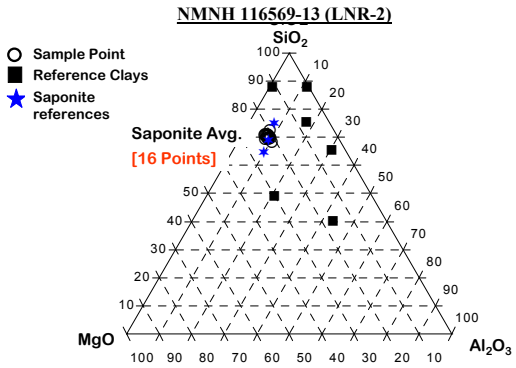

Fig. 1b. Microprobe analyses indicate the clays in Fig. 1a are consistent with saponite.

Analytical methods: A JEOL 733 electron microprobe was used to determine the chemical composition of several altered Lonar and Mistastin samples. The alteration materials were analyzed with a 15kV accelerating voltage, a 20nA beam current, counting times of 20 seconds for major element peaks, and a 5-10μm spot size. A ZAF correction was used during all microprobe analyses.

A JEOL 5800LV scanning electron microscope was used to image several alteration textures in the Lonar samples. The SEM was optimized for high-resolution imaging, which requires a 20 kV acceleration voltage, a sample current of 20 nA, a spot size of 8-10 μm, and a working distance of 8-16 mm. An automated technique for determining the abundances of trace phases was also applied to the thin sections. A Cameca 4f ion probe was used to obtain trace element data.

Results: SEM images of the altered Lonar samples show that there is abundant textural evidence for post-impact hydrothermal alteration, including classic replacement textures (**Fig. 1a, b**), and ubiquitous pockets of alteration. The abundance of the alteration phases in the Lonar sections was determined by an automated SEM technique suggesting a maximum of 5% clay (**Fig. 2**).

Microprobe results from this study were compared with several reference clays [4,5] plotted on a SiO_2, MgO, and Al_2O_3 ternary diagram. The excellent correlations suggest that the majority of the clay materials in the Lonar samples are Fe-rich saponite, with minor celadonite in some thin sections. The identification of Fe-rich saponite was confirmed by X-ray diffractometry. Both saponite and celadonite are produced during the hydrothermal alteration of basalt, typically at temperatures of 130-200°C [6]. The production of these "hydrothermal" clays was further established through geochemical modeling of the alteration process. For instance, the modeling clearly demonstrated that similar clay minerals should be produced at elevated temperatures; whereas ambient alteration appears to produce a completely different alteration assemblage.

Analytical data for the Mistastin crater samples produced somewhat different results. SEM images show alteration filling voids and possible vesicles in the impact melt samples (**Figs. 3a,b**). However, the analytical results suggest the presence of illite and glauconite (**Fig. 4**).

Conclusions and applications to Mars: We have shown that hydrothermal alteration under low water/rock ratios in impact craters can produce Fe-rich alteration phases. These results can be used to understand the behavior of hydrothermal alteration on Mars [7]. For example, an example of ion probe data

for the Lonar alteration material compared with alteration material in the Lafayette martian meteorite shows a remarkably similar pattern [8](**Fig. 5**).

Acknowledgements: Lonar crater samples provided by the Smithsonian Mineral Sciences Dept., and Mistastin samples provided by Richard Grieve. Research supported by the NASA Planetary Geology and Geophysics program (NAG5-8804, NAG 5-10143), H. Newsom P.I.

References: [1] Fredriksson, K. et al. (1973) *Science, 180,* 862. [2] Hagerty, J.J. and Newsom (2003) *Meteoritics and Planet. Sci.,* in press. [3] Fudali, R.F. et al. (1980) *Moon and Planets, 23,* 493. [4] Velde, P. et al. (1985) *Clay Minerals,* Elsevier, 427pp. [5] Newman, A.C.D. (1987) *Mineral. Soc. Mono., 6,* 480. [6] Deer, W.A. et al. (1962) *Rock Forming Minerals,* John Wiley and Sons, 270pp. [7] Nelson and Newsom, this conference. [8] Newsom et al., 2002, LPSC *XXXIII, #1577.*

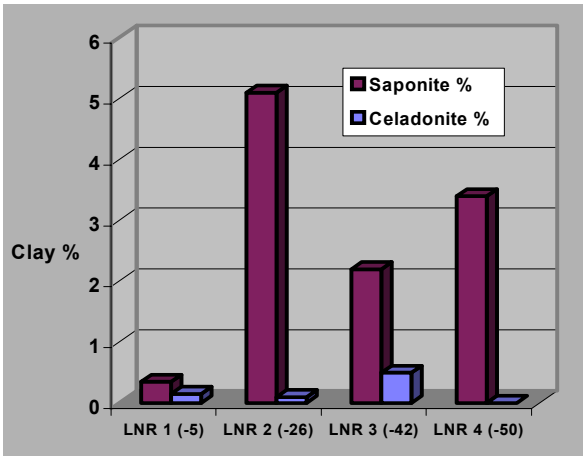

Fig. 2. Saponite abundances in Lonar thin sections determined by an automated SEM method. Typical abundances range up to 5% [2].

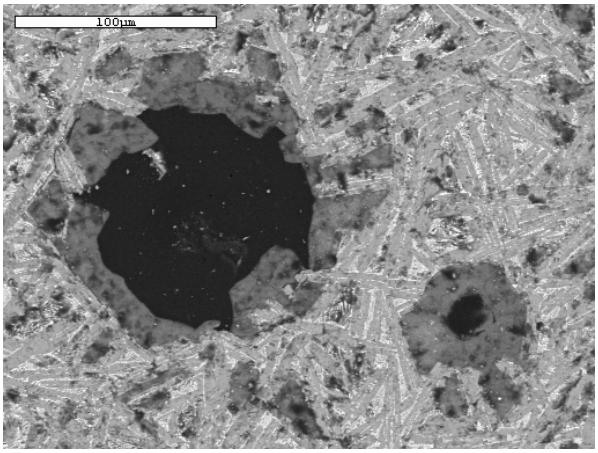

Fig. 3a. SEM image of alteration phases in Mistastin samples.

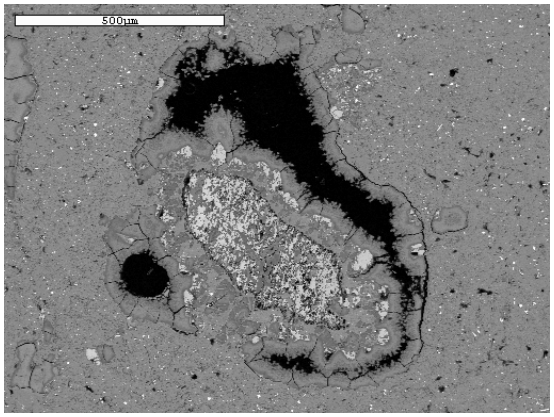

Fig. 3b. SEM image of alteration phases in Mistastin samples.

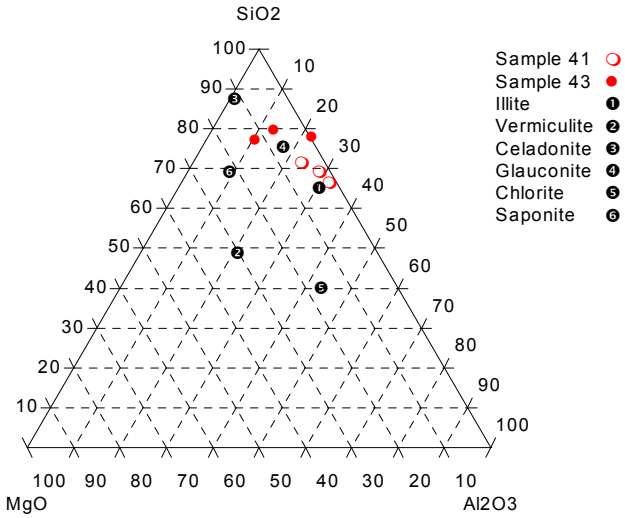

Fig. 4. Mistastin alteration materials are chemically consistent with illite and glauconite.

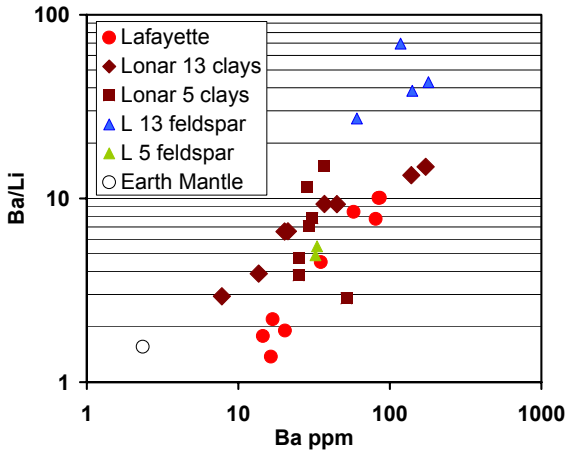

Fig. 5. Ba/Li vs. Ba diagram for preliminary SIMS data on Lonar clays and feldspar compared to similar data on Lafayette iddingsite [8]. The strikingly similar pattern suggests that similar processes have affected the terrestrial and martian basalts.

KARA IMPACT STRUCTURE, RUSSIA: RECENT DEVELOPMENTS IN PETROPHYSICAL AND GEOCHEMICAL STUDIES. T. Öhman[1], K. Lorenz[2], L. J. Pesonen[3], D. Badjukov[2], J. Raitala[4], S. Elo[5] & K. Ojala[4]. [1]Institute of Geosciences, Department of Geology, P.O. Box 3000, FIN-90014 University of Oulu, Finland (teemu.ohman@oulu.fi); [2]V.I. Vernadsky Institute of Geochemistry and Analytical Chemistry RAS, Kosigin str. 19, Moscow, 119991, Russia; [3]Department of Geophysics, P.O. Box 64, FIN-00014 University of Helsinki, Finland; [4]Planetology Group, P.O. Box 3000, FIN-90014 University of Oulu, Finland; [5]Geological Survey of Finland, Espoo Unit, P.O. Box 96, FIN-02151Espoo, Finland.

Introduction: Kara impact structure is located at 69° 05'N 64° 18'E, ~200 km north from the city of Vorkuta in arctic Russia. In the north it's bordered by the Kara Sea and in the south by the Pai-Khoi ridge. A number of studies have concentrated on the geology [e.g. 1-7], geochronology [e.g. 8-13], geochemistry [e.g. 1,3,6,14-18] and isotope systematics [19-20] of the Kara structure, but very few geophysical [1,3,16,21] and petrophysical [1,22] studies exist. The age of the impact seems to be rather well constrained at 70.3 ± 2.2 Ma [12] (most likely 68-70 Ma [13]), but the diameter(s) (~65-120 km [e.g. 16,23-25]) and the number (1-3) of craters in Kara area are still debated.

Our present study characterises the petrophysical properties of different Kara impactites and target rocks, the latter of which consist mainly of Lower Permian sedimentary rocks (sandstones, mudstones, shales) and varied Carboniferous, Devonian, Silurian and Ordovician rocks (phyllites, limestones, sandstones, diabases etc.) with Late Proterozoic schists and metamorphosed rhyolites encountered only in drill-holes [4]. We also present some new geochemical data of hydrothermal pyrites, as well as a new view into Kara using satellite imagery. In the meeting we'll present the preliminary results of our palaeomagnetic studies.

Petrophysics: We measured densities (*d*), magnetic susceptibilities (χ), intensities of natural remanent magnetization (*NRM*), Curie-points and magnetic hysteresis properties of different impactites and target rocks. The data have so far been analysed using scatter plots. More rigorous statistical analysis is underway.

Hysteresis data and Curie-point determinations of "fresh" impact glasses suggest that the main magnetic carrier is probably a low Ti-magnetite of PSD-SD domain size. However, other yet unspesified low-temperature phases are also present, and the susceptibility vs. temperature curves show alterations during the heating with new magnetic phases developing [*cf.* 22]. Hysteresis and Curie-point data also indicate that in tagamite the main carrier phase is magnetite of PSD domain size, with perhaps a minor influence from other phases.

Target rocks have a higher *d* and usually also χ, clearly differentiating them from impactites (glasses, suevites, tagamites, melt-matrix breccias) in density vs. susceptibility plots. Impactites, however, are not easily distinguished from each other. In *d* vs. χ plot only relatively fresh impact glasses with a higher χ form a somewhat tight cluster separable from other impactites. Other scatter plots, e.g. *d* vs. *NRM* or *d* vs. *Q* (Königsberger ratio), give similar results. As an approximate general trend there is an increase in *d* and χ in series: suevite – altered glass – melt-matrix breccia – tagamite – lithic breccia – target rocks. This can be seen in Figure 1, which displays the median values of *d* vs. χ for different lithologies. This trend has also been observed in many other impact structures. There is also a clear difference in *d* and χ between similar lithologies from different areas. This results not only from random errors due to limited number of samples, but also from differences in the target rocks. *NRM* and *Q* don't display as distinct relationships to different impact lithologies as *d* and χ.

Satellite imagery: Figure 2 was made utilising Landsat TM datasets (six visual to near IR channels, thermal channel omitted) from July 7th, 2000 (167/11 & 167/12). It is based on unsupervised hyper cube classification (for methods, see [26]). Although not obvious due to erosion, the innermost Kara depression can be seen as a roundish structure with a diameter of about 60 km (=D_i) in the middle left side of the image. A small intrigueing feature is the slightly curving lineament marked with arrows on the right side of the image. It's origin may have nothing to do with the impact, but we note that if one assumes this feature to be a part of an outer ring, it's diameter would be ~$2.0D_i$. Thus, Kara would fit into the oft-cited $2^{0.5}$D rule shown to hold not only for large craters and basins on other planets, but also on the Earth [27]. This feature coincides with the proposed rim of the larger Kara structure with a diameter of 110-120 km [7,21,25].

Geochemistry: We used INAA to measure the abundances of Cr, Co, Ni and Ir in hydrothermal pyrites common in the suevites. Our results differ markedly from those by Naumov [28]. Abundances of Co are roughly similar (n=12, $\bar{x}$ =23 ppm, Md=14, σ =20), but Ni-abundances vary by a factor of ~6: we found a mean Ni-content of 366 ppm (n=12, Md=270, σ =311), Naumov reports 81 ppm (n=8, Md=40, σ =99). This discrepancy is yet unexplained, but may

stem from methodological differences. Our results conserning Cr and Ir are: Cr n=13, $\bar{x}$ =11 ppm, Md=13, σ=5; Ir n=12, $\bar{x}$ =13 ppb, Md=10, σ=10. The role of possible extraterrestrial component will be discussed in the meeting.

References: [1] Maslov, M.A. (1976) *The Geologic Structure of the Kara Depression,* Ministery of Geology, Vorkuta (in Russian). [2] Masaytis, V.L. (1976) *Int. Geol. Rev., 18,* 1249-1258. [3] Maslov, M.A. (1977) *Meteoritika, 36,* 123-130 (in Russian). [4] Mashchak M.S. (1991) *Int. Geol. Rev., 33,* 423-432. [5] Mashchak M.S. (1991) *Int. Geol. Rev., 33,* 433-447. [6] Selivanovskaya T.V. et al. (1991) *Int. Geol. Rev., 33,* 448-477. [7] Nazarov M.A. et al. (1991) *LPS XXII*, 959-960. [8] Alekseev A.S. et al. (1989) *LPS XX,* 5-6. [9] Nazarov M.A. et al. (1989) *LPS XX,* 766-767. [10] Koeberl C. et al. (1990) *Geology, 18*, 50-53. [11] Kashkarov L.L. et al. (1992) *LPS XXIII,* 667-668. [12] Trieloff, M. et al. (1998) *Meteoritics & Planet. Sci., 33,* 361-371. [13] Trieloff, M. et al. (1999) *Meteoritics & Planet. Sci., 34,* 301-302. [14] Badjukov D.D. et al. (1989), *LPS XX,* 36-37. [15] Nazarov M.A. et al. (1989) *LPS XX,* 764-765. [16] Koeberl C. et al. (1990) *GSA Spec. Pap., 247,* 233-238. [17] Nazarov M.A. et al. (1990) *LPS XXI,* 849-850. [18] Badjukov D.D. et al. (1991) *LPS XXII,* 43-44. [19] Nazarov M.A. et al. (1991) *LPS XXII,* 961-962. [20] Nazarov M.A. et al. (1992), *LPS XXIII,* 973-974. [21] Badjukov D.D. et al. (2002) In: von Dalwigk I. (ed.): *8th ESF-IMPACT Workshop,* 15. [22] Badjukov D.D. et al. (1989) *LPS XX,* 34-35. [23] Nazarov M.A. et al. (1989) *LPS XX,* 762-763. [24] Masaitis V.L. (1999) *Meteoritics & Planet. Sci., 34,* 691-711. [25] Badjukov D.D. et al. (2002) *LPS XXXIII,* 1480. [26] Ojala K. et al. (2002) *36th Vernadsky-Brown Microsymposium,* MS073. [27] Pike R. (1985) *Meteoritics, 20,* 49-68. [28] Naumov M.V. (2002) In: Plado J. & Pesonen L.J. (eds.) *Impacts in Precambrian Shields,* 117-171, Springer.

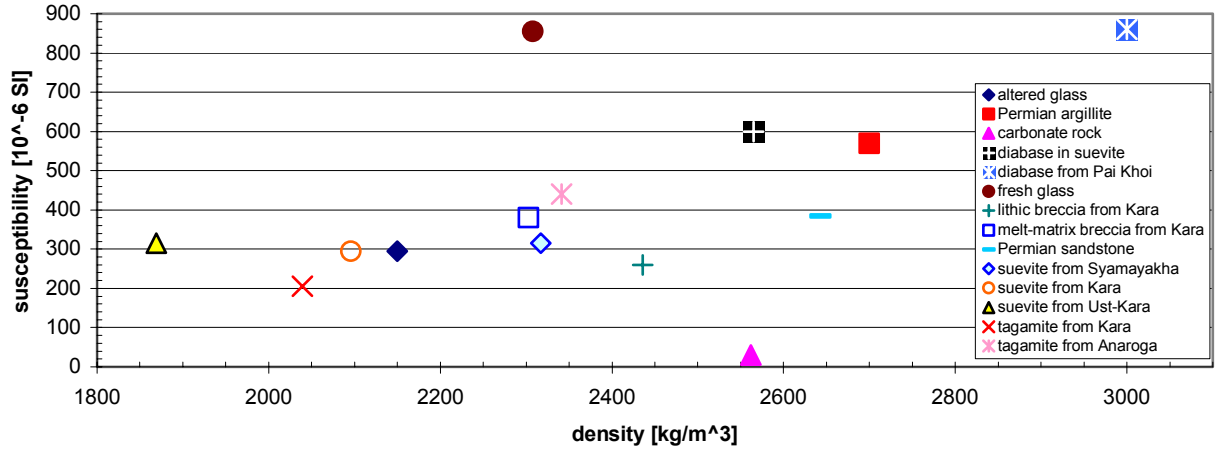

Figure 1 (above). Susceptibility as a function of density, displayed as median values (means are not used due to some outliers mainly in susceptibilities; error bars omitted for clarity). Note the difference in e.g. the suevites from different locations.

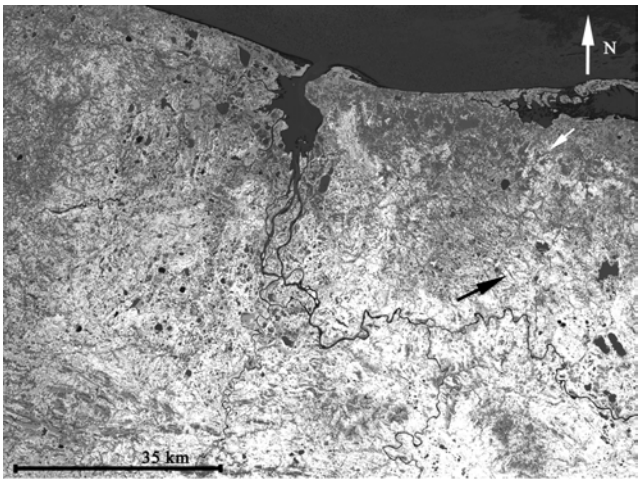

Figure 2 (left). A derivative of two Landsat TM images from the Kara region taken on July 7th 2000. Dryer water-shed ridges are shown in lighter tones. The Pai-Khoi ridge dominates the southern part and the Kara Sea the northern part of the image. Arrows mark a possibly impact-related lineament. The scale bar corresponds to 35 km.

Acknowledgements: Substantial help from academician N. Yushkin and his collegues from the Komi Geological Institute, Syktyvkar as well as from Dr. A. Bytchkov, Mr. P. Kunnas, Mr. R. Korhonen and Dipl. Natw. F. Donadini is gratefully acknowledged. This work was supported by grants from the Lappi Fund of the Finnish Cultural Foundation (the expedition), the Academy of Finland (DB), the Wihuri Foundation (TÖ) and the Väisälä Fund of the Finnish Academy of Science and Letters (TÖ).

THE SIRENTE CRATER FIELD: OUTLINE, AGE, AND EVIDENCE FOR HEATING OF THE TARGET.

J. Ormö[1], A.P. Rossi[2] and G. Komatsu[2], [1]Centro de Astrobiologia (CSIC/INTA), Ctra de Torrejón a Ajalvir, km 4 28850, Torrejón de Ardoz, Madrid, Spain (ormo@inta.es) [2]International Research School of Planetary Sciences, Universita d'Annunzio, Viale Pindaro 42, 65127 Pescara, Italy (arossi@irsps.unich.it; goro@irsps.unich.it).

Introduction: A field of small craters was recently discovered in the Apennines of central Italy [1]. The crater field is located in a mountain plain about 85 km east of Rome. No bedrock is outcropping within the Sirente plain. All the craters are developed entirely in yellowish, clayey-silty unconsolidated sediment. Coarser material and even large limestone boulders occur sporadically in the sediment. A radiocarbon dating of the target surface below the excavated material of the rim of the largest crater suggests that it formed around AD 412 ±40 [1]. The target at Sirente is almost completely devoid of quartz and no shocked quartz has been found [1]. A geochemical study together with Christian Koeberl, University of Vienna, is ongoing, but has not yet revealed any meteoritic component in samples from the craters.

Here we present preliminary results from the excavation of one of the small craters in the crater field, age dating of material interpreted as heated by the impact, as well as a more complete outline of the crater field. An exact outline of the crater field and size distribution of the craters is important when comparing with other crater fields, to estimate the physics of the atmospheric break-up, and to evaluate the magnitude of the event. An exact age is a prerequisite for any comparisons with dated historical events. It is also important to know if the small craters in the crater field are of the same age as the main crater. A contemporaneous formation of all the craters would support the impact hypothesis.

Outline of the crater field: The diameters of the small craters vary from 2 to 20 m. Some have an apparent depth of 1.5-2 m, whereas others are only shallow circular depressions. The main crater is located in one end of the crater field. It has a slightly elongated outline with a maximum diameter of 140 meters. The rim of the main crater is saddle shaped and rises at a maximum of 2.2 m above the surrounding plain. The structural uplift, commonly the main contributor for the rim formation of a simple crater, is compensated by an apparent down-warping of strata below the rim typical for craters in compactable targets [1]. The elongated shape can be a result of either low impact angle or a tight cluster of two or more craters [1].

The outline of the crater field (Fig. 1) indicates an entry from the northwest, which coincides with the length-axis of the main crater. It may indicate a highly oblique trajectory. This is, however, not supported by the steeply inclined subsurface continuation of the crater excavated in this study. Therefore, the alternative formation of the main crater by multiple impacts [1] may seem more likely. Only the most prominent craters were mapped. The exact distribution of craters is difficult to assess. The hummocky surface of the plain does probably allow some more craters to be added.

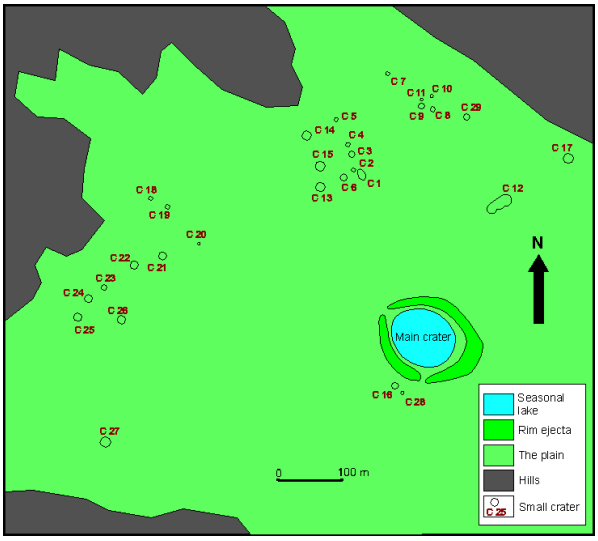

Figure 1. Outline of the crater field

Excavation of crater C8: The excavation of crater C8 (and adjacent, previously partly excavated C9, and C10 [1]) gave information on how the crater field was formed, evidence for heat in connection to the formation of the craters, and as a consequence of this heat, additional pin-pointing age data for the impact event (Table 1).

The age data suggest a contemporaneous formation of the main and small craters although with large error bars. The crater has a clear "funnel" shape with brittle rupture of the clay along its delimitation towards the host sediment (Fig. 2). Traces of disturbance of target sediment were still visible when excavation was terminated at 9 meters depth (pedogenesis of disturbed soil and injected, angular clasts (mm-cm scale) of stiff, most likely compressed, black soil along dikes in the pale clay of the host material). The excavation did not recover any macroscopic meteoritic material. Based on the excavation of the Sterlitamak crater [2], which was of the same size and formed in a similar target mate-

rial, it is likely that the excavation of C8 was not deep enough. The Sterlitamak meteorite was found at 12 meters depth.

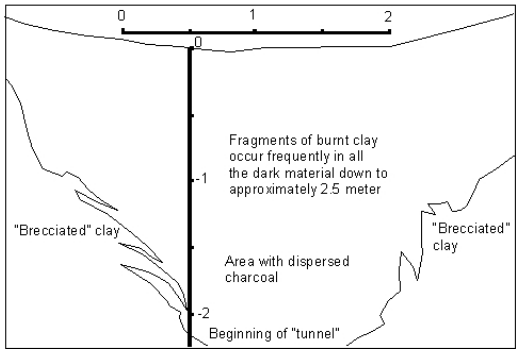

Figure 2. Section through upper part of crater C8.

At 1.8 meters depth in the lower part of the upper, bowl-shaped section of C8, there was a high content of dispersed fragments of charcoal (sample C8_coal_1.8). Small pieces of reddish, burnt clay occurred frequently in the infill of the bowl-shaped part of the crater (Fig. 3A). The largest and most solid piece was found at 2.2 meters depth (sample C8_T1_2.2). Also the material of the main crater rim show frequent, reddish-yellowish, mm-sized fragments of burnt clay (Fig. 3B). The same could not be found in reference samples from the plain.

It is questionable if an impact event of this magnitude could occur in Italy in relatively recent time without any written or oral recordings of the event. Indeed, a local oral legend from the transition time between paganism and Christianity (for the area coinciding with the dated age of the crater field) is discussed by Santilli et al. [3]. It describes how local people at the Sirente Mountain witness an approaching star that soon outshines the sun. It strikes the Sirente Mountain with such force that it generates an earthquake rupturing the local temple where a half Christian/half pagan festivity was in progress.

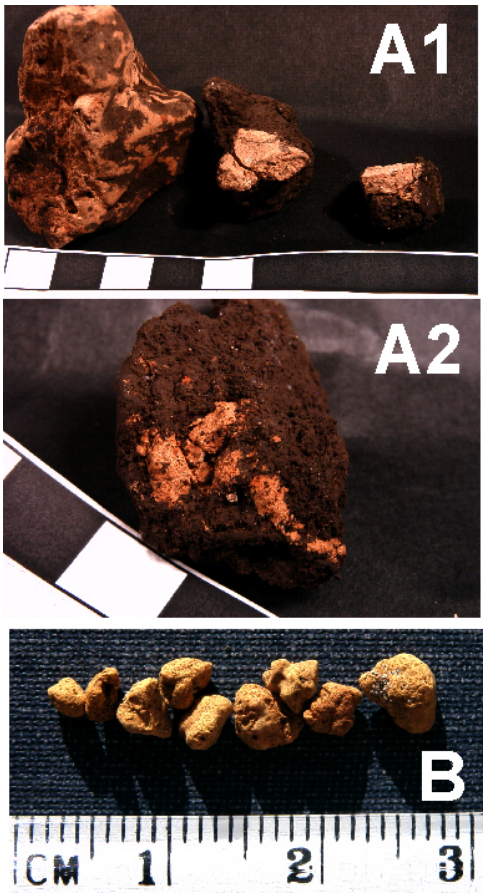

Figure 3. Heated clay from crater C8 (A1&2) and the main crater (B).

sample number	Method	Age
C8_T1_2.2	Thermoluminescence Rathgen Forschungslabor, Berlin, Germany	AD 125 ±274
C8_coal_1.8	Carbon 14, extended counting time Geochron Laboratories, U.S.A	AD 238 ± 100
DH2(1.5)	Accelerator Mass Spectrometry technique Geochron Laboratories, U.S.A	AD 412 ± 40 (from [1]).

Table 1. Age dating of samples from crater C8 and the suggested target surface below the rim ejecta of the main crater.

References: [1] Ormö J. et al. (2002) *Meteorit. Planet. Sci., 37*, 1507-1523. [2] Petaev M.I. (1992) *Astronomicheskii Vestnik, 26 (4)*, 82-99. [3] Santilli R. et al. (2003) *Antiquity* (in press).

HYPERVELOCITY IMPACT INTO CARBONATES: PROCESSES AND PRODUCTS. G. R. Osinski[1], R. A. F. Grieve[2], and J. G. Spray[1], [1]Planetary and Space Science Centre, Dept. of Geology, University of New Brunswick, 2 Bailey Drive, Fredericton, NB E3B 5A3, Canada, [2]Earth Science Sector, Natural Resources Canada, Ottawa, ON K1A 0E8, Canada. (osinski@lycos.com).

Introduction: Carbonates are present in the target rocks of approximately one third of the world's known impact structures [1]. An understanding of the response of carbonates to hypervelocity impact is needed in order to assess the effect of the impact process on these lithologies and the possible environmental influences such impacts may have had in the Earth's past [e.g., 2].

Despite the many uncertainties regarding the response of carbonates to impact, it is commonly accepted that these lithologies decompose after pressure release due to high residual temperatures and that subsequent fast back reactions trap a significant part of the gaseous species [3, 4]. This view is based, to a large extent, on experimental and theoretical studies, and computer-based simulations. However, very few detailed, systematic studies of naturally shocked carbonates have been published to date. Such studies offer the only ground-truth data on the response of carbonates to hypervelocity impact. The aim of this work is to provide an up-to-date assessment of our current understanding of hypervelocity into carbonates.

Shock experiments and thermodynamic calculations: The recent compilation by Agrinier et al. [3] indicates that shock experiments provide extremely contrasting results regarding the onset for the decomposition of carbonates. This may be due in part to differences between experimental techniques (single shock versus reverberation) and properties of the sample material (e.g., porosity) [5]. To complicate matters, substantial differences remain between experimental observations and theromodynamic calculations [3, 4, 6]. Early experimental studies suggested that calcite undergoes significant devolatilization (>10-50%) at pressures as low as 10-20 GPa [e.g., 7]. Recent shock experiments, however, coupled with petrographic and X-ray diffraction studies, suggest that substantial devolatilization of calcite and dolomite only occurs at pressures >65 GPa and >70 GPa, respectively [6, 8, 9]. Furthermore, recent dynamic loading and fast unloading experiments have produced complete shock melting of CaCO3 at pressures of ~25 GPa and temperatures of ~2700 K [8].

Phase relations of $CaCO_3$: The phase diagram for $CaCO_3$ has recently been re-evaluated in relation to shock compression and decompression by Ivanov and Deutsch [4]. The main outcome of their work has been the extension of the liquid field of $CaCO_3$. For example, isentropic release paths for calcite shocked to pressures >10 GPa first enter the liquid field, with decomposition only possible after pressures have dropped to <0.003 GPa (30 bar) at temperatures of ~1500 K. Decomposition is terminated at temperatures of <1200 K at atmospheric pressure [4]. Thus, the phase relations of $CaCO_3$ suggest that the expected result of hypervelocity impact into calcite is melting, with decomposition only occurring during post-shock cooling. Furthermore, Ivanov and Deutsch [4] also note that complex reaction kinetics, in particular the rate of diffusion, may limit the amount of CO_2 released during impact events.

Decomposition of carbonates during impact: The record in the rocks. The decomposition of carbonates releases CO_2 and produces residual solid oxides (CaO and MgO). Thus, if carbonates decompose during impact, we would expect to detect CaO and MgO in impactites within and around terrestrial impact structures. However, such residual oxides have not been documented from any terrestrial impact structure to date [e.g., 10, 11].

For impacts into limestone, this anomaly has been attributed to subsequent rapid back-reactions of CO_2 with the initially produced CaO [3]. While such reactions undoubtedly occur, it is important to note that 100% re-conversion to calcite was not achieved in any of the experiments of Agrinier et al. [3]. Re-conversion is also dependant on grain size, with a reduction in efficiency with increasing grain size [3]. Small amounts of CaO may, therefore, be expected to survive.

Is there evidence for back-reactions at terrestrial impact structures? Evidence for back-reactions has only been reported in one study by Martinez et al. [10] on naturally shocked rocks from the Haughton impact structure, Canada. These authors describe unshocked calcite present within vesicles and holes in silicate-rich impact glasses. However, these textures have been re-interpreted by several subsequent workers as evidence for carbonate-silicate liquid immiscibility [11, 12]. Thus, we suggest that impactites from Haughton should no longer be quoted as displaying unequivocal evidence for back-reactions.

The bulk of the target sequence at Haughton comprises dolomites. Unlike CaO, MgO or periclase is a stable mineral that would be expected to be preserved in impactites. Indeed, Agrinier et al. [3] note that "similar experiments with dolomite and magnesite show that residual Mg-oxides do not react significantly at the 1000 seconds time scale and may, therefore, survive as a witness of degassing in impact breccias".

Melting of carbonates during impact: The record in the rocks: Evidence for the impact melting of carbonates has now been recognized at four terrestrial

structures: (1) Meteor Crater, USA (~1.2 km diameter, ~50,000 yrs.) [13]; (2) the ~24 km Haughton impact structure, Canada (~24 km diameter, ~23 Ma) [11]; Ries impact structure, Germany (~24 km diameter, ~14.5 Ma) [12, 14]; Chicxulub impact structure, Mexico (~180 km diameter, ~65 Ma) [e.g., 15]. Evidence for this is provided by:

Carbonate-silicate liquid immiscibility. Textural evidence for liquid immiscibility between carbonates and silicate-rich impact melt glasses is common in impactites from Haughton and Ries [11, 13, 14]. This evidence includes ocellar or emulsion textures of globules of carbonate in silicate glass, sharp menisci and budding between silicate and carbonate glasses, and deformable and coalescing carbonate spheres within silicate glass. This provides unequivocal evidence for carbonates and silicate-rich glasses as initially being in the liquid state at the same time.

Quench textures. 'Fragments' of calcite displaying a distinctive feathery texture are common in proximal ejecta at Chicxulub [15]. Such textures are indicative of rapid crystallization from a melt.

Carbonate spherules. Calcite spheres occur within a variety of impactites at all the above structures. It is possible that these spheres may be mis-interpreted as vesicle fillings. However, at Haughton, the spheres occur in impactites in which there are no vesicles [11]. Vesicles are present in the Meteor Crater impactites, however, they are typically irregularly shaped and are either empty or infilled by debris [13]. It would be rather fortuitous if only the perfectly spherical vesicles were infilled by carbonate. Furthermore, no evidence for aqueous alteration has been observed in these samples, except on their surfaces [13].

Anomalous calcite compositions. Analyses of carbonates displaying textural evidence for an origin through shock melting, reveal high concentrations (up to several wt%) of Si ± Al, S [11, 13, 14]. This is in contrast to sedimentary, metamorphic, and hydrothermal calcite that contains no detectable Si or Al. This data is, however, consistent with rapid crystallization from a melt (cf., calcite in carbonatites) [11, 13, 14].

Euhedral calcite crystals and pockets of calcite in a groundmass of pyroxene. This has been observed in impactites from Meteor Crater and is hard to reconcile with an origin through alteration, but is consistent with an impact melt origin for the carbonates [13]. The melting of carbonates is also supported by the unusual composition of associated pyroxenes and olivines: coexisting Ca-rich pyroxene (diopside/wollastonite) and Mg-rich olivine (forsterite) are common in carbonatitic igneous rocks. It was also noted that these minerals are common products of the breakdown of siliceous carbonates during metamorphism [13].

Summary: Evidence for the decomposition of carbonates during hypervelocity impact has not been observed in naturally shocked rocks. For impact into limestones, this absence of evidence may be due, in part, to the re-conversion of CO_2 and CaO during fast back-reactions [e.g., 3]. Such reactions do not, however, account for the lack of MgO from the decomposition of dolomite. This may suggest that much of the MgO (and possibly CaO) is combined into silicate-rich impact melts [cf., 6]. This appears to be the case in some melts from Meteor Crater [e.g., 16] and Chicxulub [e.g., 17]. The evidence from the terrestrial impact cratering record also suggests that the impact melting of carbonates is much more common than previously thought, and that these carbonate melts are frequently preserved. This should not be surprising as the presence of extrusive carbonatites indicates that calcite can precipitate from a carbonatite magma at one atmosphere. According to the phase relations of $CaCO_3$, this should not be possible. However, it has been shown that this phenomena is due to the presence of H_2O, F, and other 'impurities' in the magma [e.g., 18]. Future studies are needed to resolves these issues and to better constrain the conditions under which carbonates may melt and/or devolatilize.

Acknowledgments: This work represents a component of the PhD thesis of GRO and was funded by the Natural Sciences and Engineering Research Council of Canada (NSERC), through research grants to JGS.

References: [1] Earth impact database (2003) http://www.unb.ca/passc/ImpactDatabase/index.htm. [2] Alvarez L. W. et al. (1980) *Science, 269,* 1095-1108. [3] Agrinier P. et al. (2001) *Geochim. Cosmochim. Acta, 65,* 2615-2632. [4] Ivanov B. A. and Deutsch A. (2002) *Phys. Earth Planet. Int., 129,* 131-143. [5] Martinez I. et al. (1995) *J. Geophys. Res., 100,* 15,465-15,476. [6] Skála R. et al. (2002) *Geol. Soc. Sp. Pap., 356,* 571-585. [7] Lange M. A. and Ahrens T. J. (1986) *Earth Planet. Sci. Lett., 83,* 1-15. [8] Langenhorst F. et al. (2000) *LPS XXXI,* #1851, CD-ROM. [9] Gupta S. C. (2002) *Earth Planet. Sci. Lett., 201,* 1-12. [10] Martinez I. et al. (1994) *Earth Planet. Sci. Lett., 121,* 559-574. [11] Osinski G. R. and Spray J. G. (2001) *Earth Planet. Sci. Lett., 194,* 17-29. [12] Graup G. (1999) *Meteor. Planet. Sci., 34,* 425-438. [13] Osinski et al. (2003) accepted for oral presentation at the 66th Annual Meteoritical Society Meeting. [14] Osinski G. R. (2003) *Meteor. Planet. Sci.,* (in review). [15] Jones et al. (2000) *Lecture notes in Earth Sciences, 91,* 343-361. [16] Hörz F. et al. (2002) *Meteorit. Planet. Sci., 37,* 501-531. [17] Sigurdsson et al. (1992) *Earth Planet. Sci. Lett., 109,* 543-560. [18] Gittins J. and Jago B. C. (1991) *Geol. Mag., 128,* 301-305.

THE NATURE OF THE GROUNDMASS OF SURFICIAL SUEVITES FROM THE RIES IMPACT STRUCTURE, GERMANY. G. R. Osinski[1], R. A. F. Grieve[2], and J. G. Spray[1], [1]Planetary and Space Science Centre, Dept. of Geology, University of New Brunswick, 2 Bailey Drive, Fredericton, NB E3B 5A3, Canada, [2]Earth Science Sector, Natural Resources Canada, Ottawa, ON K1A 0E8, Canada. (osinski@lycos.com).

Introduction: Hypervelocity impact events generate pressures and temperatures that can vaporize, melt, shock metamorphose, and/or deform a substantial volume of the target sequence. The transport and mixing of impact-metamorphosed rocks and minerals during the excavation and formation of impact craters produces a wide variety of distinctive impactites [1].

Here, we present the results of a detailed field, optical, and analytical SEM study of surficial suevites from the Ries impact structure. Suevite has been generally defined as a polymict impact breccia with a *clastic* matrix containing *fragments* of impact glass and shocked mineral and lithic clasts [1]. Our study focussed specifically on the little studied and poorly understood matrix of the surficial suevites. The results of our study reveal that the matrix is not clastic as previously thought, but contains a variety of impact melt phases.

Ries impact structure: The target rocks at the ~24 km diameter, ~14.5 Ma old Ries impact structure consist of a flat-lying sequence of predominantly Mesozoic sedimentary rocks (~470-820 m thick) that unconformably overlie Hercynian crystalline basement. The basement comprises a series of steeply inclined gneisses, amphibolites and ultrabasic rocks that are cut by a later series of granitic intrusions [2]. The Ries structure possesses a sequence of impactites, including a thick series of crater-fill rocks ('crater suevite'), various types of proximal ejecta deposits (preserved up to ~37 km radius from the crater centre), and a tektite ('moldavite') strewn field extending out to distances of 260-400 km to the east of the Ries [2]. The current study focuses on the surficial suevites.

Samples and analytical techniques: Polished thin sections were investigated using a JEOL 6400 digital scanning electron microscope (SEM) equipped with a Link Analytical eXL energy dispersive spectrometer (EDS) and Si(Li) LZ-4 Pentafet detector. Beam operating conditions were 15 kV and 2.5 nA at a working distance of 37 mm, with count times of 60-100s. The clast content and modal composition of the suevite matrix were measured on representative digital BSE images using an image analysis program (Scion Image).

Petrography of the matrix: The groundmass of surficial suevites at the Ries has previously been defined optically, as all material with a grain size <1 mm [3]. Optically unresolvable phases were termed "matrix". The analytical SEM, with its greater resolution, however, reveals that the grain size fraction <1 mm comprises a number of discrete components (with ranges of vol% in parentheses): (1) silicate mineral and lithic fragments (8.9-50.1%); (2) carbonate mineral and lithic fragments (0-12.0%); (3) angular impact glass particles (0-18.3%); (4) unshocked crystalline calcite (0-42.6%); (5) fine-grained mesostasis (1.6-70.6%) (it should be noted that our classification of mesostasis encompasses that phase which has be termed montmorillonite by earlier workers); (6) impact glass commingled with calcite and mesostasis (0-16.6%) (7) Fe-Mg-bearing plagioclase and rare garnet (0-7.5%) and pyroxene crystallites (<0.5%); (9) francolite or carbonate-hydroxy-fluoro-apatite (0-5.3%); (10) Ba-phillipsite, a Ca-K-Ba zeolite (0-34.2%).

Origin of matrix phases: Here, we redefine the "groundmass" as the fine-grained *interstitial* material that encloses fragments of shocked/unshocked target material. The matrix of the Ries surficial suevites, as defined here, comprises calcite, mesostasis, impact melt glass, crystallites (plagioclase, garnet, pyroxene), francolite, and Ba-phillipsite. The phillipsite is clearly a secondary replacement mineral and will not be considered further.

Calcite. The results of this study are consistent with the hypothesis of Graup [4] that calcite within the groundmass of surficial suevites is also an impact-generated melt phase. Evidence for this includes: (1) unequivocal evidence for liquid immiscibility between calcite, silicate-rich glass, *and* mesostasis; (2) the groundmass-supported nature of calcite-rich samples; (3) the difference in composition between carbonate clasts and groundmass calcite, including high amounts of Si (up to 0.7 wt%) in the latter; (4) the presence of isolated spheroids of pyrrhotite within calcite.

Francolite. Francolite (carbonate-hydroxy-fluoro-apatite) is only present in surficial suevites that also contain granitic fluoro-apatite-bearing clasts. Clasts of fluoro-apatite typically display euhedral to subhedral overgrowths of francolite, indicating that francolite crystallized from a melt.

Glass. Impact-generated glasses form a locally important component of the groundmass in the Ries surficial suevites. There is abundant textural evidence indicating that these glasses were not quenched until after

deposition. This evidence includes: (1) the presence of glass in the interstices between globules of mesostasis and calcite; (2) the preservation of delicate flow textures; (3) amorphous shapes with a lack of angular fragments.

Mesostasis. As noted, the 'clay' component of the groundmass from earlier investigations has been termed as mesostasis. At the SEM scale, several important characteristics of the mesostasis appear to be incompatible with a secondary hydrothermal origin. For example:

(1) A previously unrecognized feature of Ries surficial suevites is the presence of plagioclase, garnet, and pyroxene crystallites in the mesostasis. Plagioclase is invariably skeletal and typically displays hollow 'swallow tail' terminations, indicating rapid crystallization from a melt in response to high degrees of undercooling and supersaturation, and low nucleation densities [e.g., 5].

(2) Impact-generated glasses in the groundmass of Ries surficial suevites are intimately associated with mesostasis. Larger glass bodies can be seen to be deformed and streaked out into schlieren in mesostasis and vice versa. The preservation of delicate flow textures between groundmass-forming phases indicates that these glasses were liquid at the time of deposition (i.e., they were emplaced as silicate-rich melts). The same must, therefore, be true of the interfingering mesostasis.

(3) There is abundant textural evidence for liquid immiscibility between mesostasis and calcite and/or silicate-rich glass. It includes: (1) curved menisci with sharp boundaries between silicate-rich glass, calcite, and montmorillonite; (2) isolated globules of mesostasis within silicate glass and/or calcite; (3) the 'budding-off' of mesostasis globules into glass and/or calcite; (4) coalesced, or partially coalesced, mesostasis globules within silicate glass and/or calcite; (5) intermingling, but not blending, of mesostasis with calcite and silicate-rich glass; (6) highly deformed and streaked out mesostasis 'globules' associated with silicate-rich impact glass.

(4) Some vesicles (up to 16.8 vol%) in the mesostasis of surficial suevites (Fig. 4) retain a (sub-) rounded shape, whilst others have been deformed (Figs. 7a-c, 8b-d). A basic interpretation of the origin of vesicles is that the host phase (i.e., mesostasis) must have initially been a volatile-rich melt.

(5) There is considerable variation in the composition of the mesostasis (Fig. 11). Chemical heterogeneity is not typical of hydrothermal smectite group clays but is consistent in an initial impact melt origin for this phase.

(6) Even in surficial suevites that comprise >50 vol% mesostasis, silicate-rich glass fragments are typically fresh. This was noted previously by Graup [4], which led him to conclude that the preservation of these fresh glasses "simply rules out large-scale [hydrothermal] replacement processes".

Summary: The proposal of Graup [4], that calcite within the groundmass of surficial suevites crystallized from an impact-generated carbonate melt, is confirmed in this study. Silicate-rich glasses in the groundmass must also have quenched from an impact melt with the transformation to glass occurring after deposition. Crystallites, vesicles, and impact-generated glass and/or calcite intermingled with mesostasis are not compatible with a hydrothermal replacement model for the mesostasis. This work indicates that the calcite, silicate-rich glass, and mesostasis in the groundmass of the Ries surficial suevites originated as a variety of impact-generated melts.

Redefinition and classification of Ries surficial suevites? According to the suggested nomenclature of Stöffler and Grieve [1], suevite is defined as "polymict impact breccia with a *clastic* matrix/groundmass containing lithic and mineral clasts in various stages of shock metamorphism including cogenetic impact melt *clasts* which are in a glassy of crystallized state". However, the results of this study reveal that the calcite, silicate-rich glass, and mesostasis in the groundmass of Ries surficial suevites represent a series of impact-generated melts and that the bulk of these phases remained molten after deposition. Given that the Ries is the original type occurrence of "suevite", some reinterpretation of this term may be in order. Implications for the emplacement of surficial suevite will be also be discussed.

Acknowledgments: This work represents a component of the PhD thesis of GRO and was funded by the Natural Sciences and Engineering Research Council of Canada (NSERC), through research grants to JGS. Financial support for fieldwork at the Ries impact structure came from the Eugene Shoemaker Impact Cratering Award to GRO. Gisela Pösges and Michael Schieber of the Rieskratermuseum, Nördlingen, are thanked for their help during fieldwork.

References: Stöffler D. and Grieve R. A. F. (1994) *LPS XXIV,* 1347–1348. [2] Engelhardt W. v. (1990) *Tectonphys., 171*, 259-273. [3] Engelhardt W. v. and Graup G. (1984) *Geol. Rund., 73*, 447-481. [4] Graup G. (1999)) *Meteoritics & Planet. Sci., 34,* 425-438. [5] Lofgren G. (1974) *Am. J. Sci.*, *274*, 243-273.